Received 13 January 2024; revised 1 March 2024; accepted 31 March 2024. Date of publication 4 April 2024; date of current version 24 April 2024.

Digital Object Identifier 10.1109/OJCOMS.2024.3385369

Energy Buffer-Aided Wireless-Powered Relaying System for Self-Sustainable Implant WBAN

TING NING[1,2], CAN LIN[1], GUOFA CAI[1] (Senior Member, IEEE), KENGYUAN XIE[1], JIGUANG HE[3,4] (Senior Member, IEEE), CHONGWEN HUANG[5,6,7] (Member, IEEE), AND MÉROUANE DEBBAH[8] (Fellow, IEEE)

[1]School of Information Engineering, Guangdong University of Technology, Guangzhou 510006, China

[2]State Key Laboratory of Integrated Service Networks, Xidian University, Xi'an 710071, China

[3]Technology Innovation Institute, Abu Dhabi, UAE

[4]Centre for Wireless Communications, University of Oulu, 90014 Oulu, Finland

[5]College of Information Science and Electronic Engineering, Zhejiang University, Hangzhou 310027, China

[6]State Key Laboratory of Integrated Service Networks, Xidian University, Xi'an 710071, China

[7]Zhejiang-Singapore Innovation and AI Joint Research Lab and the Zhejiang Provincial Key Laboratory of Info. Proc., Commun. & Netw. (IPCAN), Zhejiang University, Hangzhou 310027, China

[8]Computer and Communication Engineering Department, College of Computing and Mathematical Sciences, Khalifa University of Science and Technology, Abu Dhabi, UAE

CORRESPONDING AUTHOR: G. CAI (e-mail: caiguofa2006@gdut.edu.cn)

This work was supported in part by the National Natural Science Foundation of China under Grant 62071129, Grant 62331023, Grant 62101492, Grant 62394292, and Grant U20A20158; in part by the China National Key Research and Development Program under Grant 2021YFA1000500 and Grant 2023YFB2904800; in part by the Zhejiang Provincial Natural Science Foundation of China under Grant LR22F010002; in part by the Zhejiang Provincial Science and Technology Plan Project under Grant 2024C01033; and in part by the Zhejiang University Global Partnership Fund.

ABSTRACT Wireless body area networks (WBANs) can provide continuous monitoring of human biological signals. Due to the limited energy of the sensors, wireless-powered system has been adopted to prolong network lifetime for implant WBANs. In this paper, we propose an energy buffer-aided wireless-powered relaying system for self-sustainable implant WBAN. The proposed system is composed of an off-body access point (AP) and many users, where an implant device is placed in body while a dual-mode wearable device with an energy buffer is attached on body for each user. In the downlink, the dual-mode wearable device simultaneously harvests energy that is stored in the energy buffer from a radio-frequency signal broadcasted by the AP and provides energy supply via wireless energy transfer to the implant device. In the uplink, the implant device uses harvested energy to transmit its collected data to the wearable device. Then the wearable device adopts the stored energy to decode and forward the data to the AP in an orthogonal multiple access way. We investigate two transmission policies for the wearable device, namely best-effort policy (BEP) and on-off policy (OOP). We derive the limiting distribution of the energy for both the BEP and OOP. Furthermore, the outage probability and average throughput of the proposed system with both the BEP and OOP are analyzed. Simulation results are presented to validate the analytical expressions and provide some useful insights.

INDEX TERMS Implant wireless body area network, best-effort policy, on-off policy, energy buffer, relaying system.

I. INTRODUCTION

WIRELESS body area networks (WBANs) that comprise low-power devices in, on, or around the human body are designed and developed to monitor physiological signals for a variety of healthcare applications in rehabilitation, sports, military and defense [2]. In particular, the

© 2024 The Authors. This work is licensed under a Creative Commons Attribution-NonCommercial-NoDerivatives 4.0 License.
For more information, see https://creativecommons.org/licenses/by-nc-nd/4.0/

implant device for implant WBAN is small in size and its battery has a limited capacity. Due to the limited capacity, scarce energy in the implant WBAN hinders its development [3]. Moreover, the implant device is usually involved with an invasive surgery for the implant WBAN [4]. Hence, it requires stringent-miniaturisation, reliability, low-power consumption, and long lifetime. The issues of the reliable data transmission and energy supply for implanted WBAN have become a research focus.

To realize high-reliability data transmission and save the energy of the implant device, relaying technologies have been introduced into the implant WBAN [5], [6], [7], [8], [9]. More specifically, the performance of relaying implant WBAN has been evaluated in terms of the bit error rate (BER) and outage probability [5]. In [6], a distributed beamforming scheme for the energy efficiency optimization has been proposed in ultra-wideband based relaying implant WBAN. In [7], a distributed reception method for the non-coherent system in the implant WBAN has been designed. However, the performance of the relaying implant WBAN is limited by the in-body link. To address this drawback, a data buffer-aided relaying framework has been proposed for implant WBAN [8]. In [9], two link-selection protocols for a data buffer-aided relaying implant WBAN has been designed and analyzed in terms of BER and average delay. Although the relaying implant WBAN can achieve the reliability and save the energy of the implant device, the energy from the battery attached to the implant device could be exhausted. Therefore the energy supply of implanted devices has received increasing attention.

To provide continuous energy self-sustaining, energy-harvesting has emerged as a promising technology to supply the implant device with permanent and sufficient power [10].[1] It can eliminate the need for bulky batteries or drastically reduce the size of their rechargeable batteries [12], which can further bring implant miniaturization to millimeter scales [13]. This method is to make the implant device energy self-sustaining by scavenging the energy from a variety of sources available in the ambient environment or the body itself [14]. However, opportunistic energy harvesting from the human body such as biochemical [15] and biomechanical [16] energy or renewable energy sources such as solar [17] and heat energy [18] is in general intermittent and uncontrollable. In contrast, wireless power transfer (WPT) system is partially controllable and can provide a perpetual energy source and continuous operation of the low-power devices [19], [20], [21], [22]. Near-field based WPT systems have been adopted to charge and communicate with the biomedical implant devices [23], [24]. However, the distance between the power supply and the implant device cannot exceed few centimeters. Radio frequency (RF)-based WPT system can extend the distance between the power supply and the implant device, which can achieve a few meters [11]. In [11], RF-based WPT system for the implant device has been developed. In [25], the electromagnetic compatibility of RF-based WPT system for the wearable and implant devices has been investigated. Recently, the performance of WPT system for the implant WBAN has been investigated in [26]. Based on above works, it is interesting to combine relaying with WPT systems in WBAN.

To integrate the advantages of relaying and WPT systems, relaying WPT system has been applied into the WBAN [27], [28], [29], [30], [31]. More specifically, in [27], spectral efficiency of the relaying WPT-based WBAN system has been studied over a block fading channel. In [28], an optimal strategy for the relaying WPT-based WBAN system has been proposed to achieve the maximum throughput. In [29], a relay selection protocol for the relaying WPT-based WBAN system with data buffer has been designed. In [30], a cooperative communication framework for the WPT-based WBAN system with full duplex has been constructed and its throughput maximization problem has been investigated under the limited delay. Recently, a dynamic weights algorithm for the relaying WPT-based system has been designed in [31]. In such system, the relay and sensors collect energy from the AP and use the harvested energy to transmit information to the AP by using time division multiple access. However, in these works [27], [28], [29], [30], [31], all of them utilize relaying and WPT in WBAN, but energy harvesting nodes of these systems use a harvest-use (HU) architecture, which does not buffer the energy for use in future time slots and limits system performance. Moreover, they do not manage the energy. To solve this problem, an energy buffer can be equipped at the energy-harvesting nodes, which can use the harvest-store-use (HSU) architecture [32] and the energy is managed. Recently, two online simple policies, i.e., best-effort policy (BEP) and on-off policy (OOP), have been proposed for the energy buffer aided point-to-point WPT system [33]. The proposed system in this paper adds relaying to the energy buffer-aided point-to-point WPT system, and the BEP and OOP are re-modeled and derived. In such system, a discrete-time continuous-state Markov chain model is used to model the energy buffer accurately. The performance of a two-hop network with energy buffer-aided relay has been analyzed in [34], while an incremental relay has been adopted to improve the spectral efficiency in [35]. In [36], [37], the performance of a two-hop network with energy buffer-aided source has been analyzed. Hence, introducing energy buffer at the relay or/and the source can significantly improve the performance of the wireless-powered relaying systems. However, in these works [34], [35], [36], [37], which manage the energy in the energy buffer, the energy is collected from the environment. The source of energy in the environment is unstable and random. To address this problem, the proposed system in this paper obtains the energy from the RF signals broadcasted by the AP.

[1]Charging implanted devices is a big challenge in practical application scenarios. The emergence of in-vivo networking (IVN) can help to solve this issue. IVN can integrate coherently-incoherent beamforming into a complete system that optimally provides power and communicates with deep-tissue biosensors and bioactuators [11].

With the above motivation, in this paper, we propose an energy buffer-aided wireless-powered relaying system for self-sustainable implant WBAN, which includes an off-body access point (AP) and one group of users. For each user, an implant device and a dual-mode wearable device are equipped in and on human body, respectively.[2] Because the implant device is generally implanted in the tissue of the human, it requires miniaturization and free battery [11], [41]. To ensure the reliable power supply and safety, the energy of the implant device is provided via the wearable device due to the uncontrollable AP.[3] Moreover, the wearable device on the human body can attach to the battery to store the energy from the AP. Due to these requirements, the implant device and the wearable device adopt HU and HSU architectures, respectively.

The main results and contributions of this paper are summarized as follows.

1) An energy buffer-aided wireless-powered relaying system for implant WBAN is proposed. The proposed system not only can provide reliable energy supply for the implant device that is not dependent on the AP and transmit the collected data of the implant device without any external power supply, but also can ensure the safety for the human health.
2) In the proposed system, the dual-mode wearable device adopts BEP and OOP to manage the energy in the energy buffer. The limiting distributions of the energy in the energy buffer for both the BEP and OOP are derived by using a continuous state space Markov chain. Furthermore, the outage probability and average throughput of the proposed system with the BEP and OOP are analyzed.
3) Simulations are conducted to verify the accuracy of the theoretical analysis and demonstrate that both the BEP and OOP possess better performance compared with the existing battery-less relaying system. Furthermore, some useful insights are given to show the design rules for the implant WBAN.

The remainder of this paper is organized as follows. In Section II, we show the system model of the proposed system. In Section III, we derive the limiting distribution of the energy buffer. We analyze the performance of the proposed system in Section IV. The results and discussion are presented in Section V. Section VI concludes the paper.

[2]In WBAN standard [5], [38], [39], [40], the implant device works at the Medical Implant Communication Service (MICS) frequency band (402-405 MHz), while the wearable device works at the Industrial, Scientific and Medical (ISM) frequency band (2360-2400 MHz). Hence, the wearable device is designed in dual-mode.

[3]In fact, the battery of the wearable device can be easily replaced or can be recharged. When human body is not within the scope of the AP, the wearable device can keep providing the energy for the implant device. In addition, to avoid electromagnetic emissions that could be harmful for the human health, the transmitted power of the relay should be below the specific absorption rate (SAR) limit [24]. However, the existing implant WBAN systems, for example [11], [26], mainly consider the harvested energy from the uncontrollable AP.

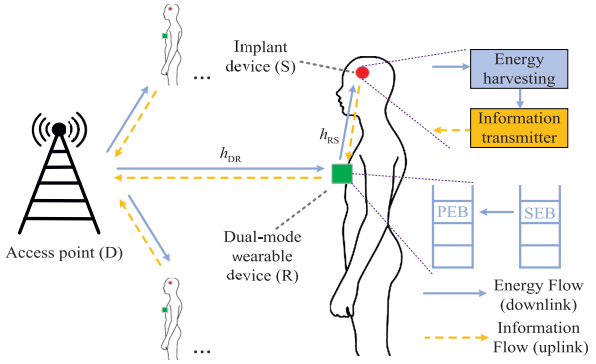

FIGURE 1. An energy buffer-aided wireless-powered relaying system for implant WBAN.

Notations: Bold lowercase letters denote vectors (e.g., $\boldsymbol{a}$), while bold capital letters represent matrices (e.g., $\boldsymbol{A}$). $\mathbb{E}(x)$ is the expectation of x, $\Re\{x\}$ denotes the real part of x, and $j=\sqrt{-1}$ is the imaginary unit. $\mathbf{x}^T$ denotes the transpose of vector $\mathbf{x}$. $\mathbb{P}\{x\}$ denotes the probability of x, and $\mathbf{1}$ denotes an all-one vector.

II. SYSTEM MODEL

This section first describes the proposed system and its transmission interval, and then presents phase I, phase II, and phase III of the interval.

We consider a wireless-powered relaying system for implant WBAN,[4] as shown in Fig. 1, which includes an off-body AP (D) and one group of uniformly distributed users. Each user has an implant device (S) and a dual-mode wearable device (R) that are placed in and on body, respectively. In the considered system, D is equipped with a power supply, whereas S and R are powered wirelessly. R is equipped with an energy buffer (e.g., a rechargeable battery or a large super-capacitor) that can store and release energy. It should be noted that because the batteries cannot charge and discharge at the same time, the harvested energy is stored in a secondary energy buffer (SEB), and the energy is drawn for the transmission from a primary energy buffer (PEB) [34]. In the downlink, R uses HSU architecture to harvest energy that will be stored in the energy buffer from a RF signal broadcasted by D. Moreover, because S is often implanted in the tissue of the human, it requires miniaturization and free battery. To ensure the reliable power supply and the safety, R provides energy supply via wireless energy transfer to S, which adopts the HU architecture (e.g., the super-capacitors based architectures [45]). Moreover, in the uplink, S transmits the collected information by using the harvested energy to R. Noted that, in this phase, the interference between users generally cannot happen due to the deep fading. In addition, R can adopt the stored energy to decode and forward the data from the users to the AP simultaneously in an orthogonal multiple access (OMA) way.

[4]In fact, the proposed system can be used for wireless deep brain stimulation (DBS), pacemaker, spinal cord stimulators, etc. [42], [43], [44]. In addition, implanted devices that are swallowed or injected into the body can be used to decode brain circuits, deliver drugs, or monitor vital signs within the body [11].

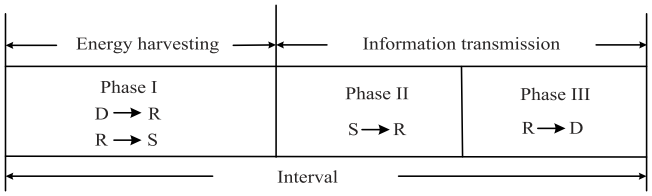

FIGURE 2. Wireless power transfer and information transmission at each interval.

Two OMA methods, i.e., frequency division multiple access (FDMA) or time division multiple access (TDMA), can be adopted for multiple WBANs to eliminate the interference. In this sense, we only consider an AP and a user in the following.

The wireless power transfer and information transmission at each interval is shown in Fig. 2. Let $B(i)$ denote the energy level in the energy buffer at the i-th interval, P_{RS} denote the transmit power from R to S, and M denote a constant power that is used for information transmission from R to D. At R, two different policies, i.e., BEP and OOP, are considered. Considering the $(i+1)$-th interval, the basic principle is described as follows. In phase I, D sends the RF signal to R, and R harvests the energy that will be stored in the energy buffer. At this time, the energy level in the energy buffer is $B(i+1)$. In this phase, for the BEP, when $B(i+1) > P_{\mathrm{RS}}$, R transmits RF signal to S and S harvests the energy, otherwise, R remains silent and waits for the next interval. For the OOP, when $B(i+1) \geq M + P_{\mathrm{RS}}$, R transmits RF signal to S and S harvests the energy, otherwise, R remains silent and waits for the next interval. In phase II, S uses the harvested energy to transmit its collected data to R. In phase III, R uses the stored energy to decode and forward the data to D. In this phase, for the BEP, if the energy in the buffer is enough, R transmits the information to D with a constant power M, otherwise, R transmits with a lower power. For the OOP, R always transmits the information to D with a constant power M. The detail information of the signal model is given as follows.

In phase I, D transmits RF signal to R and R transmits RF signal to S. The received signal at R can be given by

$$y_{\mathrm{DR}} = \sqrt{\ell P_{\mathrm{D}}} h_{\mathrm{DR}} s_1 + n_{\mathrm{R}}, \tag{1}$$

where P_{D} is the transmit power at D, h_{DR} is the Nakagami-m fading channel from D to R,[5] s_1 is the energy-carrying signal with zero mean and unit power, $\ell = \frac{1}{(d_{\mathrm{RD}})^{\alpha}}$ denotes the path loss factor between D and R, d_{RD} is the distance between D and R, α is the path loss exponent, and n_{R} is complex additive Gaussian white noise (AWGN) with zero mean and variance $N_{0,\mathrm{R}}$. The harvested energy in the i-th interval is given by $X(i) = \eta \ell P_{\mathrm{D}} |h_{\mathrm{DR}}|^2$, where η is the energy-harvesting efficiency and $|h_{\mathrm{DR}}|^2$ follows Gamma distribution with an integer shape parameter m and the scale parameter $\Omega_{\mathrm{DR}} = \mathbb{E}(|h_{\mathrm{DR}}|^2)$. In addition, the harvested energy $X(i)$ is an independent and identically distributed (i.i.d.) stationary and ergodic process with mean $\bar{X} = \eta \ell P_{\mathrm{D}} \Omega_{\mathrm{DR}}$.

[5]Generally, the channel gain from D to R can be modeled by the log-normal and Nakagami-m distributions [5], [46]. In fact, Nakagami-m distribution can be used to represent the log-normal distribution in an accurate manner [47], [48], [49].

TABLE 1. Parameters for path loss models for different tissues.

Implant body	$P_L(d_0)$	n	σ_p
Deep tissue	47.14	4.26	7.85
Near surface	49.81	4.22	6.81

Moreover, the received signal at S can be written as

$$y_{\mathrm{RS}} = \sqrt{P_{\mathrm{RS}}} h_{\mathrm{RS}} s_1 + n_{\mathrm{S}}, \tag{2}$$

where h_{RS} is the log-normal fading channel from R to S, and n_{S} is also complex AWGN with zero mean and variance $N_{0,\mathrm{S}}$. The statistical path loss between S and R is expressed as

$$P_L(d) = P_L(d_0) + 10n\log_{10}\frac{d_{\mathrm{SR}}}{d_0} + p, \tag{3}$$

where d_{SR} is the distance of SR link, p follows normal distribution with zero mean and variance σ_p^2, $P_L(d_0)$ is the path loss at a reference distance $d_0 = 50$ mm, n is the path loss exponent, and these parameters are shown in Table 1 [5]. The harvested energy at S is given by $P_{\mathrm{S}} = \eta P_{\mathrm{RS}} |h_{\mathrm{RS}}|^2$, where $|h_{\mathrm{RS}}|^2$ follows log-normal distribution and it uses a linear EH model.[6] According to [5], the probability density function (PDF) of $x = |h_{\mathrm{RS}}|^2 = 10^{-\frac{P_L(d)}{10}}$ can be given by

$$q(x) = \frac{1}{\sqrt{2\pi\sigma_s^2}x} e^{-\frac{(\ln(x)-\ln(a))^2}{2\sigma_s^2}}, \tag{4}$$

where $\sigma_s = \frac{\sigma_p \ln(10)}{10}$ and $a = 10^{-\frac{P_L(d_0)+10n\log_{10}\frac{d_{\mathrm{SR}}}{d_0}}{10}}$.

In phase II, the harvested energy P_{S} is used to transmit the collected data s_2 from S to R. The received signal at R can be written as

$$y_{\mathrm{SR}} = \sqrt{P_{\mathrm{S}}} h_{\mathrm{SR}} s_2 + n_{\mathrm{R}}, \tag{5}$$

where $h_{\mathrm{SR}} = h_{\mathrm{RS}}$ due to the channel reciprocity. The SNR at R can be defined as $\gamma_{\mathrm{SR}} = \frac{P_{\mathrm{S}}|h_{\mathrm{SR}}|^2}{N_{0,\mathrm{R}}}$, which follows log-normal distribution.

In phase III, R first decodes the received signal y_{SR} from S, and then forwards the estimated data $\hat{s}_2$ to D. The received signal at D can be given by

$$y_{\mathrm{RD}} = \sqrt{\ell P_{\mathrm{RD}}} h_{\mathrm{RD}} \hat{s}_2 + n_{\mathrm{D}}, \tag{6}$$

where P_{RD} is the transmit power at R, $h_{\mathrm{RD}} = h_{\mathrm{DR}}$ due to the channel reciprocity, and n_{D} is also complex AWGN with zero mean and variance $N_{0,\mathrm{D}}$. Hence, $\Omega_{\mathrm{RD}} = \mathbb{E}(|h_{\mathrm{RD}}|^2) = \Omega_{\mathrm{DR}}$. The SNR at D can be defined as $\gamma_{\mathrm{RD}} = \frac{\ell P_{\mathrm{RD}}|h_{\mathrm{RD}}|^2}{N_{0,\mathrm{D}}}$, which follows Gamma distribution.

[6]In practical situations, a nonlinear EH model is usually considered [50], [51]. However, due to the increased complexity of the energy expression with nonlinear models, it becomes more difficult to calculate the effective distribution of signal-to-noise ratios (SNRs) and derive outage probability for the proposed system. To simplify the analysis, a linear EH model [52] is adopted in this paper. The above nonlinearity issues will be left as our future investigation.

According to the above principle, the update equation of the energy buffer for the BEP can be given by

$$B(i+1) = \min(B(i)+X(i), K), B(i) \le P_{\mathrm{RS}} \tag{7a}$$
$$B(i+1) = \min(X(i), K), P_{\mathrm{RS}} < B(i) \le M + P_{\mathrm{RS}} \tag{7b}$$
$$B(i+1) = \min(B(i) - P_{\mathrm{RS}} - M + X(i), K), B(i) > M + P_{\mathrm{RS}}, \tag{7c}$$

while for the OOP it can be written as

$$B(i+1) = \min(B(i)+X(i), K), B(i) \le M + P_{\mathrm{RS}} \tag{8a}$$
$$B(i+1) = \min(B(i) - P_{\mathrm{RS}} - M + X(i), K), B(i) > M + P_{\mathrm{RS}}. \tag{8b}$$

where K denotes the buffer size of the energy buffer and $\min(a, b)$ returns the minimum of a and b.

III. LIMITING DISTRIBUTION OF THE ENERGY BUFFER

A. LIMITING DISTRIBUTION OF THE BEP

Let $g(x)$ on $(0, \infty)$ be the limiting PDF of the stored energy. $f(x)$ and $F(x)$ are the PDF and cumulative distribution function (CDF) of $\{X(i)\}$, respectively. Consider the buffer of size $K = l(M + P_{\mathrm{RS}}) + \Delta$, where $l \in \mathbb{Z}^+$, $\mathbb{Z}^+$ denotes the positive integers and $P_{\mathrm{RS}} \le \Delta < M + P_{\mathrm{RS}}$. We set $B(i+1) = x$ and $B(i) = u$, thus (7) can be written as

$$x = \min(u + X(i), K), u \le P_{\mathrm{RS}} \tag{9a}$$
$$x = \min(X(i), K), P_{\mathrm{RS}} < u \le M + P_{\mathrm{RS}} \tag{9b}$$
$$x = \min(u - P_{\mathrm{RS}} - M + X(i), K), u > M + P_{\mathrm{RS}}. \tag{9c}$$

Referred to [33], using (9), $g(x)$ is computed as

$$g(x) = \begin{cases} \int_{u=0}^{x} f(x-u)g(u)du + f(x)\int_{u=P_{\mathrm{RS}}}^{M+P_{\mathrm{RS}}} g(u)du \\ + \int_{u=M+P_{\mathrm{RS}}}^{M+P_{\mathrm{RS}}+x} f(x-u+P_{\mathrm{RS}}+M)g(u)du, \ 0 \le x < P_{\mathrm{RS}} \\ \int_{u=0}^{P_{\mathrm{RS}}} f(x-u)g(u)du + f(x)\int_{u=P_{\mathrm{RS}}}^{M+P_{\mathrm{RS}}} g(u)du \\ + \int_{u=M+P_{\mathrm{RS}}}^{M+P_{\mathrm{RS}}+x} f(x-u+P_{\mathrm{RS}}+M)g(u)du, \ P_{\mathrm{RS}} \\ \le x < K - M - P_{\mathrm{RS}} \\ \int_{u=0}^{P_{\mathrm{RS}}} f(x-u)g(u)du + f(x)\int_{u=P_{\mathrm{RS}}}^{M+P_{\mathrm{RS}}} g(u)du \\ + \int_{u=M+P_{\mathrm{RS}}}^{K} f(x-u+P_{\mathrm{RS}}+M)g(u)du \\ + \pi(K) f(x-K+P_{\mathrm{RS}}+M), \ K - M - P_{\mathrm{RS}} \le x < K, \end{cases} \tag{10}$$

where the probability of a full buffer $\pi(K)$ is given by

$$\pi(K) = \frac{1}{1 - F(M + P_{\mathrm{RS}})} \left[\int_{u=0}^{P_{\mathrm{RS}}} F(K-u)g(u)du + F(K)\int_{u=P_{\mathrm{RS}}}^{M+P_{\mathrm{RS}}} g(u)du + \int_{u=M+P_{\mathrm{RS}}}^{K} F(K-u+P_{\mathrm{RS}}+M)g(u)du \right], \tag{11}$$

Because $X(i)$ follows Gamma distribution, its PDF and CDF are given by $f(x) = \frac{\lambda^m}{\Gamma(m)} x^{m-1} e^{-\lambda x}$, and $F(x) = e^{-\lambda x} \sum_{r=0}^{m-1} \frac{(\lambda x)^r}{r!}$, respectively, where $\lambda = \frac{m}{\bar{X}}$ and $m \in \{1, 2, \ldots, \}$. To find the performance at optimal M, $\delta = \frac{M + P_{\mathrm{RS}}}{\bar{X}}$ is defined as the ratio of transmission energy threshold to $\bar{X}$. The complementary cumulative distribution function (CCDF) is written as $\bar{F}(x) = 1 - F(x)$. Hence, $g(x)$ can be calculated as (II), where $n = 0, \ldots, l', l' = \begin{cases} l-1, & \Delta = 0 \\ l, & \Delta \ne 0 \end{cases}$ $C_1(x) = x^{m-1} + \frac{1}{m} \sum_{k=0}^{m-1} \Re\{(\lambda e^{j\eta_k})^{-(m-1)} e^{\lambda x e^{j\eta_k}} \gamma(m, \lambda x e^{j\eta_k})\}$, $C_2(x, v) = x^{m+v} + \frac{1}{m} \sum_{k=0}^{m-1} \Re\{(\lambda e^{j\eta_k})^{-(m+v)} e^{\lambda x e^{j\eta_k}} \gamma(m+v+1, \lambda x e^{j\eta_k})\}$, $\eta_k = \frac{2\pi k}{m}$, and α_r can be obtained by solving $\boldsymbol{\alpha} + \boldsymbol{A}\boldsymbol{\alpha} = \mathbf{1}$. The s-row and r-column expression for $\boldsymbol{A}$ is given by (13), as shown at the bottom of the next page. The derivation of (II) is provided in Appendix A.

B. LIMITING DISTRIBUTION OF THE OOP

We consider the buffer of size $K = l(M + P_{\mathrm{RS}})$ with $l \in \{3, 4, \ldots, \}$. $f(x)$ and $F(x)$ are the same as these for BEP. Similarly, (8) can be written as

$$x = \min(u + X(i), K), u \le M + P_{\mathrm{RS}} \tag{15a}$$
$$x = \min(u - P_{\mathrm{RS}} - M + X(i), K), u > M + P_{\mathrm{RS}}. \tag{15b}$$

Using (15), $g(x)$ is computed as

$$g(x) = \begin{cases} \int_{u=M+P_{\mathrm{RS}}}^{M+P_{\mathrm{RS}}+x} f(x-u+P_{\mathrm{RS}}+M)g(u)du \\ + \int_{u=0}^{x} f(x-u)g(u)du, \qquad 0 \le x < M + P_{\mathrm{RS}} \\ \int_{u=M+P_{\mathrm{RS}}}^{M+P_{\mathrm{RS}}+x} f(x-u+P_{\mathrm{RS}}+M)g(u)du \\ + \int_{u=0}^{M+P_{\mathrm{RS}}} f(x-u)g(u)du, M + P_{\mathrm{RS}} \\ \le x < K - M - P_{\mathrm{RS}} \\ \int_{u=0}^{M+P_{\mathrm{RS}}} f(x-u)g(u)du \\ + \int_{u=M+P_{\mathrm{RS}}}^{K} f(x-u+P_{\mathrm{RS}}+M)g(u)du \\ + \pi(K) f(x-K+P_{\mathrm{RS}}+M), K - M - P_{\mathrm{RS}} \\ \le x < K, \end{cases} \tag{16}$$

where $\pi(K)$ is given by

$$\pi(K) = \frac{1}{1 - F(M + P_{\mathrm{RS}})} \left[\int_{u=0}^{M+P_{\mathrm{RS}}} F(K-u)g(u)du + \int_{u=M+P_{\mathrm{RS}}}^{K} F(K-u+P_{\mathrm{RS}}+M)g(u)du \right]. \tag{17}$$

Referring to [33], $g(x)$ can be further calculated as (34), where $n = 0, \ldots, l-2$, and $C_3(x, v) = x^{m+v} + \frac{1}{m} \sum_{k=0}^{m-1} \Re\{(\lambda e^{j\eta_k})^{-(m+v)} e^{\lambda x e^{j\eta_k}} \gamma(m+v+1, \lambda x e^{j\eta_k})\}$.

IV. PERFORMANCE ANALYSIS

In this section, the outage probability and average throughput of the proposed system are derived. The outage probability for the proposed system is derived as

$$P_{\text{out}} = \mathbb{P}\{\min(\gamma_{\text{SR}}, \gamma_{\text{RD}}) < \gamma_{\text{thr}}\}$$
$$= 1 - \mathbb{P}\{\gamma_{\text{SR}} > \gamma_{\text{thr}}\}\mathbb{P}\{\gamma_{\text{RD}} > \gamma_{\text{thr}}\}$$
$$= 1 - \big(1 - P_{\text{out\_SR}}\big)\big(1 - P_{\text{out\_RD}}\big)$$
$$= P_{\text{out\_SR}} + P_{\text{out\_RD}} - P_{\text{out\_SR}}P_{\text{out\_RD}}, \quad (18)$$

where $\gamma_{\text{thr}} = 2^{R_t} - 1$ and R_t in bits per channel use (bpcu) denotes the transmission rate, without loss of generality, we

$$g(x) = \begin{cases} g_p(x) = e^{-\lambda x}\sum_{r=0}^{m-1}\frac{\alpha_r}{r}\Bigg[\sum_{z=0}^{l-1}\lambda^m e^{-\lambda(z(M+P_{\text{RS}})+P_{\text{RS}})}\sum_{v=0}^{(z+1)m-1-r}\frac{(z(M+P_{\text{RS}})+P_{\text{RS}}-K)^{(z+1)m-1-r-v}}{((z+1)m-1-r-v)v(m-1)} \\ \times\lambda^{(z+1)m-1-r-v}\gamma(v+1,\lambda M)C_1(x) - \sum_{z=1}^{l-1}\lambda^m e^{-\lambda(z(M+P_{\text{RS}})+P_{\text{RS}})}\sum_{v=0}^{zm-1}\frac{(z(M+P_{\text{RS}})+P_{\text{RS}}-K)^{zm-1-v}}{(zm-1-v)v(m-1)} \\ \times\lambda^{zm-1-v}\gamma(v+1,\lambda M)C_1(x) + \lambda^m e^{-\lambda(l(M+P_{\text{RS}})+P_{\text{RS}})}\sum_{v=0}^{(l+1)m-1-r}\frac{(l(M+P_{\text{RS}})+P_{\text{RS}}-K)^{(l+1)m-1-r-v}}{((l+1)m-1-r-v)v(m-1)} \\ \times\lambda^{(l+1)m-1-r-v}\gamma(v+1,\lambda(K-(l(M+P_{\text{RS}})+P_{\text{RS}})))C_1(x) - \lambda^m e^{-\lambda(l(M+P_{\text{RS}})+P_{\text{RS}})} \\ \times\sum_{v=0}^{lm-1}\frac{(l(M+P_{\text{RS}})+P_{\text{RS}}-K)^{lm-1-v}}{(lm-1-v)v(m-1)}\lambda^{lm-1-v}\gamma(v+1,\lambda(K-(l(M+P_{\text{RS}})+P_{\text{RS}})))C_1(x) \\ +\sum_{z=0}^{l-1}\lambda^{(z+2)m-r}e^{-\lambda(z+1)(M+P_{\text{RS}})}\sum_{v=0}^{(z+1)m-1-r}\frac{((z+1)(M+P_{\text{RS}})-K)^{(z+1)m-1-r-v}}{((z+1)m-1-r-v)(m+v)}C_2(x,v) \\ -\sum_{z=1}^{l-1}\lambda^{(z+1)m}e^{-\lambda(z+1)(M+P_{\text{RS}})}\sum_{v=0}^{zm-1}\frac{((z+1)(M+P_{\text{RS}})-K)^{zm-1-v}}{(zm-1-v)(m+v)}C_2(x,v)\Bigg], \quad 0\le x<P_{\text{RS}} \quad (12a) \\ g_n(x) = e^{-\lambda x}\sum_{r=0}^{m-1}\frac{\alpha_r}{r}\Bigg[\sum_{z=0}^{n}\lambda^{(z+1)m-r}e^{-z\lambda(M+P_{\text{RS}})}\frac{(z(M+P_{\text{RS}})+x-K)^{(z+1)m-1-r}}{((z+1)m-1-r)} \\ -\sum_{z=1}^{n}\lambda^{zm}e^{-z\lambda(M+P_{\text{RS}})}\frac{(z(M+P_{\text{RS}})+x-K)^{zm-1}}{(zm-1)}\Bigg], [K-(n+1)(M+P_{\text{RS}})]^+\le x<K-n(M+P_{\text{RS}}), \quad (12b) \end{cases}$$

$$A_{sr} = \frac{1}{r!}\Bigg[\sum_{z=0}^{l-1}e^{-\lambda(z(M+P_{\text{RS}})+P_{\text{RS}})}\sum_{v=0}^{(z+1)m-1-r}\frac{(z(M+P_{\text{RS}})+P_{\text{RS}}-K)^{(z+1)m-1-r-v}}{((z+1)m-1-r-v)!v!}\lambda^{(z+1)m-1-r-v}\gamma(v+1,\lambda M)$$
$$\times\big(\lambda^m H_1 - K^s\lambda^s - \lambda^{m+s}F_1(s)\big) - \sum_{z=1}^{l-1}e^{-\lambda(z(M+P_{\text{RS}})+P_{\text{RS}})}\sum_{v=0}^{zm-1}\frac{(z(M+P_{\text{RS}})+P_{\text{RS}}-K)^{zm-1-v}}{(zm-1-v)!v!}\lambda^{zm-1-v}$$
$$\times\gamma(v+1,\lambda M)\big(\lambda^m H_1 - K^s\lambda^s - \lambda^{m+s}F_1(s)\big) + e^{-\lambda(l(M+P_{\text{RS}})+P_{\text{RS}})}\sum_{v=0}^{(l+1)m-1-r}\frac{(l(M+P_{\text{RS}})+P_{\text{RS}}-K)^{(l+1)m-1-r-v}}{((l+1)m-1-r-v)!v!}$$
$$\times\lambda^{(l+1)m-1-r-v}\gamma(v+1,\lambda(K-(l(M+P_{\text{RS}})+P_{\text{RS}})))\big(\lambda^m H_1 - K^s\lambda^s - \lambda^{m+s}F_1(s)\big) - e^{-\lambda(l(M+P_{\text{RS}})+P_{\text{RS}})}$$
$$\times\sum_{v=0}^{lm-1}\frac{(l(M+P_{\text{RS}})+P_{\text{RS}}-K)^{lm-1-v}}{(lm-1-v)!v!}\lambda^{lm-1-v}\gamma(v+1,\lambda(K-(l(M+P_{\text{RS}})+P_{\text{RS}})))\big(\lambda^m H_1 - K^s\lambda^s - \lambda^{m+s}F_1(s)\big)$$
$$+\sum_{z=0}^{l-1}\lambda^{(z+2)m-r}e^{-\lambda(z+1)(M+P_{\text{RS}})}\sum_{v=0}^{(z+1)m-1-r}\frac{((z+1)(M+P_{\text{RS}})-K)^{(z+1)m-1-r-v}}{((z+1)m-1-r-v)!}\big(H_2(v)-\lambda^s F_2(v,s)\big)$$
$$-\sum_{z=1}^{l-1}\lambda^{(z+1)m}e^{-\lambda(z+1)(M+P_{\text{RS}})}\sum_{v=0}^{zm-1}\frac{((z+1)(M+P_{\text{RS}})-K)^{zm-1-v}}{(zm-1-v)!}\big(H_2(v)-\lambda^s F_2(v,s)\big)$$
$$+\sum_{z=0}^{l}e^{-\lambda(z(M+P_{\text{RS}})+P_{\text{RS}})}\sum_{v=zm}^{(z+1)m-1-r}\frac{(\lambda(z(M+P_{\text{RS}})+P_{\text{RS}}-K))^v}{v!} + K^s\lambda^s\sum_{z=0}^{l-1}\lambda^{zm}e^{-\lambda(z+1)(M+P_{\text{RS}})}$$
$$\times\sum_{v=0}^{s}\binom{s}{v}K^{-v}v!\left(\lambda^{m-r}\frac{((z+1)(M+P_{\text{RS}})-K)^{(z+1)m-r+v}}{((z+1)m-r+v)!} - \frac{((z+1)(M+P_{\text{RS}})-K)^{zm+v}}{(zm+v)!}\right)\Bigg]. \quad (13)$$

set $R_t = R_{\mathrm{SR}} = R_{\mathrm{RD}}$, where R_{SR} is the transmission rate of the SR link and R_{RD} is the transmission rate of the RD link, $P_{\mathrm{out\_SR}}$ and $P_{\mathrm{out\_RD}}$ are the outage probabilities of the SR link and RD link, respectively. The average throughput of the considered system can be obtained as $T = R_t(1 - P_{\mathrm{out}})$.

According to the CDF of the log-normal distribution, the outage probability $P_{\mathrm{out\_SR}}$ can be calculated as

$$P_{\mathrm{out\_SR}} = \mathbb{P}\{\gamma_{\mathrm{SR}} < \gamma_{\mathrm{thr}}\} = \frac{1}{2} + \frac{1}{2}\mathrm{erf}\left(\frac{\ln(\gamma_{\mathrm{thr}}) - \mu}{2\sigma_s}\right), \quad (19)$$

where $\mathrm{erf}(x) = \frac{2}{\sqrt{\pi}}\int_0^x e^{-t^2}dt$, $\mu = \ln(\frac{\eta P_{\mathrm{RS}} a^2}{N_{0,\mathrm{R}}})$.

In the following, the derivation of $P_{\mathrm{out\_RD}}$ for both the BEP and OOP is given.

A. BEP

For the BEP, $P_{\mathrm{out\_RD}}$ can be obtained as

$$P_{\mathrm{out\_RD}} = P_M P_{\mathrm{out}}\big|_{P_{\mathrm{RD}}=M} + P_{\mathrm{out}}\big|_{B(i)<P_{\mathrm{RS}}} + \int_{P_{\mathrm{RS}}}^{M+P_{\mathrm{RS}}} \mathbb{P}\left\{\frac{[x - P_{\mathrm{RS}}]^+ \ell |h_{\mathrm{RD}}|^2}{N_{0,\mathrm{D}}} < \gamma_{\mathrm{thr}}\right\} g(x)dx, \quad (20)$$

where $P_M = \mathbb{P}\{P_{\mathrm{RD}} = M\}$ is defined as the probability that the RD link transmits with power M, $P_{\mathrm{out}}|_{P_{\mathrm{RD}}=M}$. is the outage probability that the transmit power $P_{\mathrm{RD}} = M$, $P_{\mathrm{out}}|_{B(i)<P_{\mathrm{RS}}}$. is the probability that the stored energy at R is less than P_{RS}.

1) DERIVATION OF P_M

P_M is calculated as

$$\begin{aligned} P_M &= \int_{M+P_{\mathrm{RS}}}^{K} g(x)dx + \pi(K) \\ &= \sum_{r=0}^{m-1}\frac{\alpha_r}{r!}\sum_{z=0}^{l-1} e^{-\lambda(z+1)(M+P_{\mathrm{RS}})} \\ &\quad \times \sum_{v=zm}^{(z+1)m-1-r} \frac{(\lambda((z+1)(M+P_{\mathrm{RS}}) - K))^v}{v!}. \end{aligned} \quad (21)$$

2) DERIVATION OF $P_{\mathrm{OUT}}|_{P_{\mathrm{RD}}=M}$.

$P_{\mathrm{out}}|_{P_{\mathrm{RD}}=M}$ can be computed as

$$\begin{aligned} P_{\mathrm{out}}\big|_{P_{\mathrm{RD}}=M} &= \mathbb{P}\left\{\frac{\ell M |h_{\mathrm{RD}}|^2}{N_{0,\mathrm{D}}} < \gamma_{\mathrm{thr}}\right\} \\ &= \mathbb{P}\left\{|h_{\mathrm{RD}}|^2 < \frac{\gamma_{\mathrm{thr}} N_{0,\mathrm{D}}}{\ell M}\right\} \\ &= \frac{\gamma\left(m, \frac{E}{M}\right)}{\Gamma(m)}, \end{aligned} \quad (22)$$

where $E = \frac{m\gamma_{\mathrm{thr}} N_{0,\mathrm{D}}}{\ell \Omega_{\mathrm{RD}}}$ and $\gamma(m,x) = (m-1)!(1 - e^{-x}\sum_{n=0}^{m-1}\frac{x^n}{n!})$.

3) CLOSED FORM OF THE INTEGRAL IN (20)

Since the transmission is also allowed when the stored energy is more than P_{RS} but less than $M + P_{\mathrm{RS}}$, it is necessary to solve the last term in (20). It can be calculated as

$$\begin{aligned} &\int_{P_{\mathrm{RS}}}^{M+P_{\mathrm{RS}}} \mathbb{P}\left\{\frac{[x - P_{\mathrm{RS}}]^+ \ell |h_{\mathrm{RD}}|^2}{N_{0,\mathrm{D}}} < \gamma_{\mathrm{thr}}\right\} g(x)dx \\ &= \int_{P_{\mathrm{RS}}}^{M+P_{\mathrm{RS}}} \frac{\gamma\left(m, \frac{E}{x-P_{\mathrm{RS}}}\right)}{\Gamma(m)} g(x)dx \\ &= \int_{P_{\mathrm{RS}}}^{M+P_{\mathrm{RS}}} g(x)dx - \int_{P_{\mathrm{RS}}}^{M+P_{\mathrm{RS}}} e^{-\frac{E}{x-P_{\mathrm{RS}}}} \sum_{v=0}^{m-1} \frac{\left(\frac{E}{x-P_{\mathrm{RS}}}\right)^v}{v!} g(x)dx \\ &= 1 - P_M - P_{\mathrm{out}}\big|_{B(i)<P_{\mathrm{RS}}} \\ &\quad - \sum_{v=0}^{m-1}\frac{E^v}{v!} \underbrace{\int_{P_{\mathrm{RS}}}^{M+P_{\mathrm{RS}}} \frac{e^{-\frac{E}{x-P_{\mathrm{RS}}}}}{(x-P_{\mathrm{RS}})^v} g(x)dx}_{I_t}. \end{aligned} \quad (23)$$

In (23), I_t can be obtained as

$$\begin{aligned} I_t = \sum_{r=0}^{m-1}\frac{\alpha_r}{r!}\Bigg[&\sum_{z=0}^{l''} \lambda^{(z+1)m-r} e^{-\lambda(z(M+P_{\mathrm{RS}})+P_{\mathrm{RS}})} D^{(z+1)m-r-v} \\ &\times N\left(v, \frac{E}{D}, \lambda D, \frac{K - (z(M+P_{\mathrm{RS}})+P_{\mathrm{RS}})}{D}, (z+1)m - r - 1\right) \\ &- \sum_{z=1}^{l''} \lambda^{zm} e^{-\lambda(z(M+P_{\mathrm{RS}})+P_{\mathrm{RS}})} D^{zm-v} \end{aligned}$$

$$g(x) = \begin{cases} g_{l-1}(x) = e^{-\lambda x}\sum_{r=0}^{m-1}\frac{\alpha_r}{r}\Bigg[\sum_{z=0}^{l-2}\lambda^{(z+2)m-r}e^{-\lambda(z+1)(M+P_{\mathrm{RS}})}\sum_{v=0}^{(z+1)m-1-r}\frac{((z+1)(M+P_{\mathrm{RS}})-K)^{(z+1)m-1-r-v}}{((z+1)m-1-r-v)(m+v)}C_3(x,v) \\ -\sum_{z=1}^{l-2}\lambda^{(z+1)m}e^{-\lambda(z+1)(M+P_{\mathrm{RS}})}\sum_{v=0}^{zm-1}\frac{((z+1)(M+P_{\mathrm{RS}})-K)^{zm-1-v}}{(zm-1-v)(m+v)}C_3(x,v)\Bigg], \quad 0 \le x < M+P_{\mathrm{RS}} \quad (14a) \\ g_n(x) = e^{-\lambda x}\sum_{r=0}^{m-1}\frac{\alpha_r}{r}\Bigg[\sum_{z=0}^{n}\lambda^{(z+1)m-r}e^{-z\lambda(M+P_{\mathrm{RS}})}\frac{(z(M+P_{\mathrm{RS}})+x-K)^{(z+1)m-1-r}}{((z+1)m-1-r)} - \sum_{z=1}^{n}\lambda^{zm}e^{-z\lambda(M+P_{\mathrm{RS}})} \\ \times\frac{(z(M+P_{\mathrm{RS}})+x-K)^{zm-1}}{(zm-1)}\Bigg], \quad [K-(n+1)(M+P_{\mathrm{RS}})]^+ \le x < K-n(M+P_{\mathrm{RS}}) \quad (14b) \end{cases}$$

$$\times N\left(v, \frac{E}{D}, \lambda D, \frac{K-(z(M+P_{\mathrm{RS}})+P_{\mathrm{RS}})}{D}, zm-1\right)\Bigg], \quad (24)$$

where $l'' = \begin{cases} l-1, & \Delta < P_{\mathrm{RS}} \\ l, & \Delta > P_{\mathrm{RS}} \end{cases}$, $D = \begin{cases} M, & z < l \\ \Delta - P_{\mathrm{RS}} & z = l \end{cases}$, and $N(v,a,b,c,d) = \int_0^1 \frac{e^{-\frac{a}{x}-bx}}{x^v} \frac{(x-c)^d}{d!} dx$.

Substituting (21), (22)|, and (23) into (20), the outage probability $P_{\mathrm{out\_RD}}$ can be obtained by

$$P_{\mathrm{out\_RD}} = P_M P_{\mathrm{out}}\big|_{P_{\mathrm{RD}}=M} + 1 - P_M - \sum_{v=0}^{m-1} \frac{E^v}{v!} I_t. \quad (25)$$

Hence, combining (19) and (26) with (18), the outage probability of the considered system for the BEP can be obtained. Also, the corresponding average throughput can be calculated.

B. OOP

The outage probability $P_{\mathrm{out\_RD}}$ for the OOP is given by

$$P_{\mathrm{out\_RD}} = P_M P_{\mathrm{out}}\big|_{P_{\mathrm{RD}}=M} + 1 - P_M, \quad (26)$$

where $P_{\mathrm{out}}|_{P_{\mathrm{RD}}=M}$. is the same as the BEP and

$$\begin{aligned} P_M &= \int_{M+P_{\mathrm{RS}}}^{K} g(x)dx + \pi(K) \\ &= \sum_{r=0}^{m-1} \frac{\alpha_r}{r!} \sum_{z=0}^{l-2} e^{-\lambda(z+1)(M+P_{\mathrm{RS}})} \\ &\quad \times \sum_{v=zm}^{(z+1)m-1-r} \frac{(\lambda((z+1)(M+P_{\mathrm{RS}})-K))^v}{v!}. \end{aligned} \quad (27)$$

Substituting (27) and (22) into (26), the outage probability $P_{\mathrm{out\_RD}}$ can be obtained. Similarly, combining (19) and (26) with (18), the outage probability of the considered system for the OOP can be obtained. Also, the corresponding average throughput can be calculated.

V. RESULTS AND DISCUSSIONS

In this section, we present simulated results to validate the analytical expressions and obtain some insights. To verify the superiority of the BEP and OOP, a buffer-less policy (BLP)[7] is adopted as a benchmark scheme [31], where R is not equipped with energy buffer. Figs. 3 and 4 illustrate the effects of distances d_{RD} and d_{SR} on the amount of harvested energy at R and S. As d_{RD} (or d_{SR}) increases, the amount of energy harvested by R (or S) decreases. In addition, as P_{D} (or P_{RS}) increases, the amount of energy harvested by R (or S) increases. From Fig. 3, it can be seen that when $P_{\mathrm{D}} = 1$ W and $d_{\mathrm{RD}} = 1$ m, the energy collected by R is enough for the usage of the relay. To ensure that the transmitted power of the relay is below the SAR limit, the value of P_{RS} should be not larger than 10 mW. From Fig. 4, it is observed

[7]BLP uses all the energy collected in one time slot to transmit information [33].

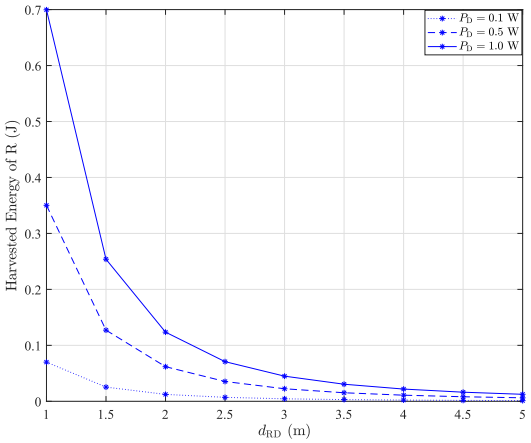

FIGURE 3. Effect of distance d_{RD} on the amount of the harvested energy at R, where $d_{\mathrm{SR}} = 50$ mm, and $R_t = 2$ BPCU.

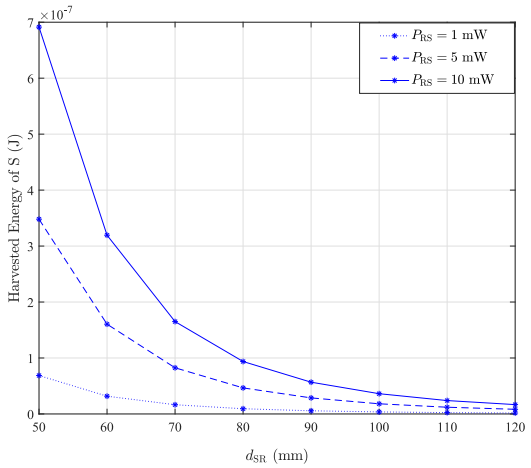

FIGURE 4. Effect of distance d_{SR} on the amount of the harvested energy at S, where $d_{\mathrm{RD}} = 1$ m, and $R_t = 2$ BPCU.

that the energy collected by S is less than 25 uW, which avoids electromagnetic emissions that could be harmful for the human health [40]. For safety reasons, the simulation parameters are shown in Table 2.

Fig. 5 shows the outage probability versus δ for the BEP, OOP and BLP with different values of R_t, where $m = 2$, $l = 4$, and $d_{\mathrm{RD}} = 1$ m. First, it can be observed that the theoretical curves well match with the simulated curves, which validates the accuracy of the theoretical analysis. Moreover, there is an optimal δ that achieves the best performance for the BEP and OOP. When $\delta \leq 0.4$, the same performance of the BEP and OOP are obtained because the energy in the buffer is always beyond the threshold $M + P_{\mathrm{RS}}$. When $\delta > 0.4$, the BEP has better performance than the OOP. The reason is that the energy in the buffer is less than $M + P_{\mathrm{RS}}$. Thus, the outage occurs for the OOP while it does not for the BEP. Furthermore, with the increase of R_t, the performance of the BEP, OOP, and BLP are worse. In addition, it is observed that the BEP and OOP with the optimal value of δ may obtain better performance than the BLP.

TABLE 2. Simulation parameters.

Parameter	Value
Conversion efficiency	$\eta = 0.85$
Path loss exponent	$\alpha = 2.5$
Noise power at R	$N_{0,\mathrm{R}} = -124$ dBm
Noise power at D	$N_{0,\mathrm{D}} = 0$ dBm
DR transmit power	$P_{\mathrm{D}} = 1$ W
RS transmit power	$P_{\mathrm{RS}} = 10$ mW
Integer shape parameter	$m = 2$

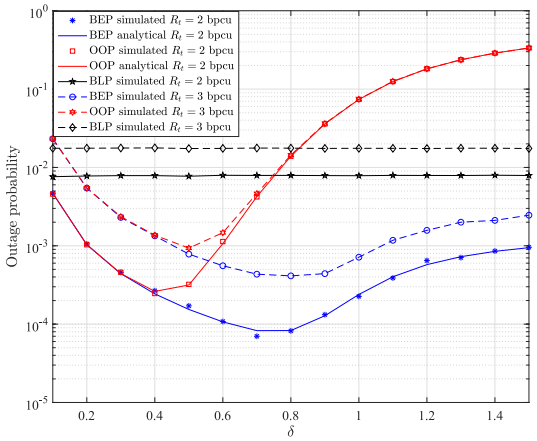

FIGURE 5. Outage probabilities versus δ for the BEP, OOP and BLP with different values of R_t, where $d_{\mathrm{SR}} = 50$ mm, $d_{\mathrm{RD}} = 1$ m, and $l = 4$.

Figs. 6, 7, and 8 depict the outage probability versus δ for the BEP, OOP and BLP with different values of d_{SR}, d_{RD}, and P_{RS}, respectively. First, it can be seen from Fig. 6 that with the increase of d_{SR} performance of the three policies are worse due to the serious path loss of the SR link. In particular, when the implant device is implanted very deep, the BLP obtains better performance than the BEP and OOP. The reason is that there is not enough energy in the implant device. To ensure the better performance and provide self-sustainable capability of the proposed system, it can increase the value of P_{RS}, as shown in Fig. 8. Second, it is observed from Fig. 7 that when the AP is far away from the human body, performance of three policies are worse due to serious path loss of the RD link. On the other words, when the human body is not within the scope of the AP, the two systems cannot provide the self-sustainable capability. Fortunately, the proposed system can start the backup battery of the wearable device to wirelessly power the implant device, thus it can keep working. In this sense, the proposed system is not dependent on the AP compared with the existing system with the BLP that the harvested energy is from the AP.

Fig. 9 illustrates the outage probability versus δ for the BEP and OOP with different values of l. With the increase of l (i.e., buffer size K of the energy buffer), the performance of the BEP and OOP significantly improves. For the low buffer size, the BEP has better performance than the OOP

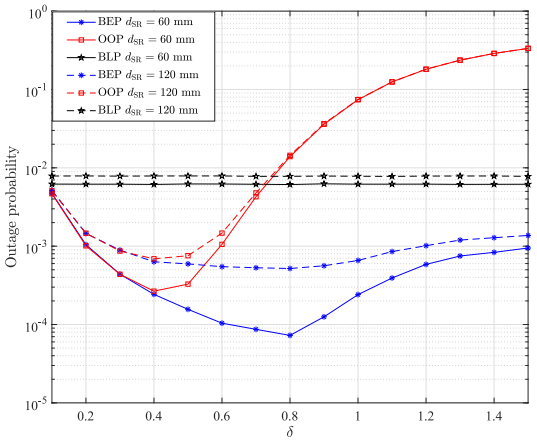

FIGURE 6. Outage probability versus δ for the BEP, OOP and BLP with different values of d_{SR}, where $R_t = 2$ BPCU, $d_{\mathrm{RD}} = 1$ m, and $l = 4$.

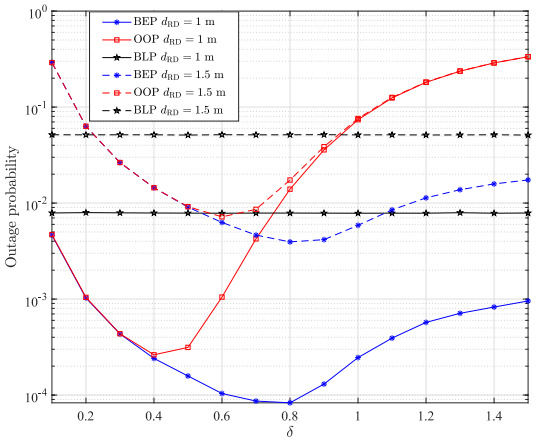

FIGURE 7. Outage probability versus δ for the BEP, OOP and BLP with different values of d_{RD}, where $d_{\mathrm{SR}} = 50$ mm, $R_t = 2$ BPCU, and $l = 4$.

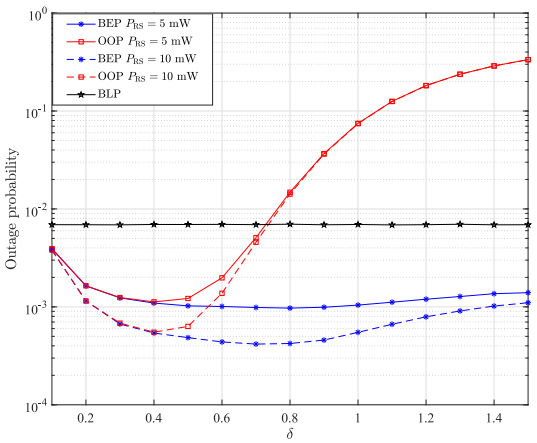

FIGURE 8. Outage probability versus δ for the BEP, OOP and BLP with different values of P_{RS}, where $d_{\mathrm{SR}} = 120$ mm, $d_{\mathrm{RD}} = 1$ m, $R_t = 2$ BPCU, and $l = 4$.

at the optimal value of δ. The reason is that the OOP policy is not allowed to transmit at a low power and makes the probability of buffer overflow higher. For the large buffer

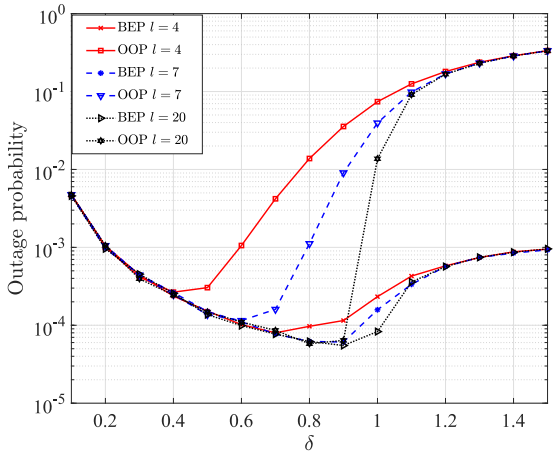

FIGURE 9. Outage probability versus δ for the BEP and OOP with different values of l, where $R_t = 2$ bpcu, $d_{SR} = 50$ mm, and $d_{RD} = 1$ m.

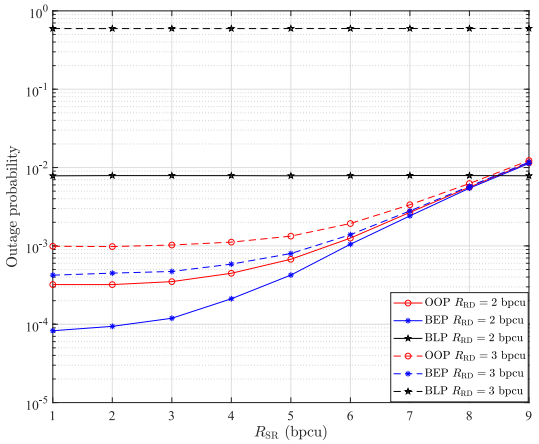

FIGURE 10. Outage probability versus R_{SR} for the BEP and OOP with different values of R_{RD}, where $\delta = 0.7$, $d_{SR} = 50$ mm, and $d_{RD} = 1$ m.

size, performance of the OOP is close to or the same as that of the BEP at the optimal value of δ.

Fig. 10 shows the outage probability versus R_{SR} for the BEP and OOP with different values of R_{RD}, where $\delta = 0.7$, $d_{SR} = 50$ mm, and $d_{RD} = 1$ m. Firstly, it can be seen that the outage performance of all three policies becomes worse as R_{SR} increases. Secondly, the increase of R_{RD} also makes the outage performance worse. This is because the bandwidth of the system cannot meet the requirement of the transmission rate as the transmission rate increases, thus making the outage performance worse. Besides, the outage performance of BEP is better than that of OOP and BLP.

Fig. 11 depicts the average throughput versus R_t for the BEP, OOP and BLP, where $m = 2$, $l = 4$, and $d_{RD} = 1$ m. The average throughput of the BEP and OOP, with the optimal value of δ is obtained for each R_t. For low transmission rates, although the two policies have better outage performance at a small value of R_t, they have low average throughput. For medium transmission rates, the average throughput of the BEP is superior to that of the OOP and BLP. For high transmission rates, the average throughput

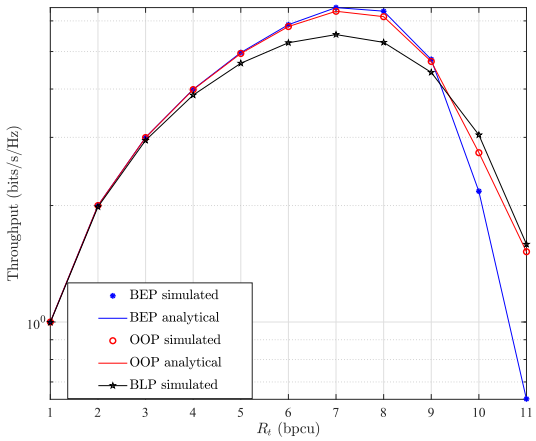

FIGURE 11. Average throughput versus R_t for the BEP, OOP and BLP, where $l = 4$, $d_{SR} = 50$ mm, and $d_{RD} = 1$ m.

of the BLP is close to that of the OOP, which is superior to that of the BEP.

Remark 1: From the above discussions, it is clear that the change for each parameter causes a consequent change in the system performance. First, it can be seen from Fig. 5, 6, and 7 that the system outage performance deteriorates with the increase of R_t, d_{SR}, and d_{RD}, respectively. In order to obtain better system performance, the transmission rate R_t of the system should not be set too large, and the distance between the AP and the user should not be too far. Moreover, it can be seen from Fig. 8 and 9 that with the increase of P_{RS} and l, the system performance becomes better. An appropriate increase in P_{RS} and l can improve the system outage performance. This is because the increase of P_{RS} is harmful to the human body and its value cannot exceed 10 mW. In addtion, the increase of l makes the buffer capacity increase, and the device is configured with larger buffer, which will cause a certain burden and increase the complexity of the system.

VI. CONCLUSION

In this paper, we have proposed an energy buffer aided wireless-powered relaying system for implant WBAN. The proposed system can provide the self-sustainable capability and the energy supply of the implant device is not dependent on the AP compared with the existing systems adopting BLP. Moreover, we have derived the limiting distribution of the energy for both the BEP and OOP. Furthermore, we have analyzed the outage probability and average throughput of the proposed system with the BEP and OOP. Simulation results show that both the BEP and OOP with optimal value of δ not only can provide better outage performance than that of the BLP, but also have high average throughput than that of the BLP for medium transmission rates. In addition, when the implant device is implanted very deep, the BEP and OOP can obtain better performance than the BLP by increasing the buffer size. Thanks to the aforementioned advantages, the proposed system can be considered as a promising candidate

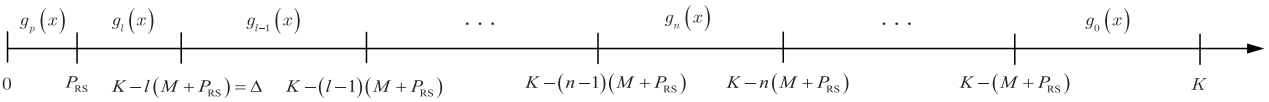

FIGURE 12. Segmentation of $g(x)$ for the BEP.

for self-sustainable implant WBAN applications. In future work, a data buffer can be added to the system model, where the tradeoff between the delay and BER will be further studied.

APPENDIX
DERIVATION OF $G(X)$ FOR THE BEP

Substituting $f(x)$, $F(x)$ and $\bar{F}(x)$ into (10) and (11), $g(x)$ and $\pi(K)$ can be obtained and given in (23) and (29), as shown at the bottom of the page, respectively. Let $I_1(r) = \int_{u=0}^{P_{\mathrm{RS}}} (K-u)^r e^{\lambda u} g(u)du$, $I_2(r) = K^r \int_{u=P_{\mathrm{RS}}}^{M+P_{\mathrm{RS}}} g(u)du$, $I_3(r) = \int_{u=M+P_{\mathrm{RS}}}^{K} (K-u+P_{\mathrm{RS}}+M)^r e^{-\lambda(M+P_{\mathrm{RS}}-u)} g(u)du$, $\alpha_r = \lambda^r[I_1(r) + I_2(r) + I_3(r) + (M+P_{\mathrm{RS}})^r \pi(K) e^{-\lambda(M+P_{\mathrm{RS}}-K)}]$, $g(x)$ can be given in (23) and $\pi(K) = e^{-\lambda K} \sum_{r=0}^{m-1} \frac{\alpha_r}{r!}$.

$$
g(x) = \begin{cases}
\dfrac{\lambda^m e^{-\lambda x}}{(m-1)} \left[\displaystyle\int_{u=0}^{x} (x-u)^{m-1} e^{\lambda u} g(u)du + x^{m-1} \int_{u=P_{\mathrm{RS}}}^{M+P_{\mathrm{RS}}} g(u)du \right. \\
\left. + \displaystyle\int_{u=M+P_{\mathrm{RS}}}^{M+P_{\mathrm{RS}}+x} (x-u+P_{\mathrm{RS}}+M)^{m-1} e^{-\lambda(M+P_{\mathrm{RS}}-u)} g(u)du \right], & 0 \le x < P_{\mathrm{RS}} \quad (28a) \\
\dfrac{\lambda^m e^{-\lambda x}}{(m-1)} \left[\displaystyle\int_{u=0}^{P_{\mathrm{RS}}} (x-u)^{m-1} e^{\lambda u} g(u)du + x^{m-1} \int_{u=P_{\mathrm{RS}}}^{M+P_{\mathrm{RS}}} g(u)du \right. \\
\left. + \displaystyle\int_{u=M+P_{\mathrm{RS}}}^{M+P_{\mathrm{RS}}+x} (x-u+P_{\mathrm{RS}}+M)^{m-1} e^{-\lambda(M+P_{\mathrm{RS}}-u)} g(u)du \right], & P_{\mathrm{RS}} \le x < K-M-P_{\mathrm{RS}} \quad (28b) \\
\dfrac{\lambda^m e^{-\lambda x}}{(m-1)} \left[\displaystyle\int_{u=0}^{P_{\mathrm{RS}}} (x-u)^{m-1} e^{\lambda u} g(u)du + x^{m-1} \int_{u=P_{\mathrm{RS}}}^{M+P_{\mathrm{RS}}} g(u)du + \pi(K)(x-K+P_{\mathrm{RS}}+M)^{m-1} e^{-\lambda(M+P_{\mathrm{RS}}-K)} \right. \\
\left. + \displaystyle\int_{u=M+P_{\mathrm{RS}}}^{K} (x-u+P_{\mathrm{RS}}+M)^{m-1} e^{-\lambda(M+P_{\mathrm{RS}}-u)} g(u)du \right], & K-M-P_{\mathrm{RS}} \le x < K. \quad (28c)
\end{cases}
$$

$$
\pi(K) = \frac{e^{-\lambda K}}{1 - e^{-\lambda(M+P_{\mathrm{RS}})} \sum_{r=0}^{m-1} \frac{(\lambda(M+P_{\mathrm{RS}}))^r}{r!}} \left[\sum_{r=0}^{m-1} \frac{\lambda^r}{r!} \left(\underbrace{\int_{u=0}^{P_{\mathrm{RS}}} (K-u)^r e^{\lambda u} g(u)du}_{I_1(r)} + \underbrace{K^r \int_{u=P_{\mathrm{RS}}}^{M+P_{\mathrm{RS}}} g(u)du}_{I_2(r)} \right. \right.
$$

$$
\left. \left. + \underbrace{\int_{u=M+P_{\mathrm{RS}}}^{K} (K-u+P_{\mathrm{RS}}+M)^r e^{-\lambda(M+P_{\mathrm{RS}}-u)} g(u)du}_{I_3(r)} \right) \right]. \quad (29)
$$

As shown in Fig. 11, $g_n(x) \triangleq g(x)$, $[K-(n+1)(M+P_{\mathrm{RS}})]^+ \le x < K-n(M+P_{\mathrm{RS}})$, where $n = 0, \ldots, l'$, $l' = \begin{cases} l-1, & \Delta = 0 \\ l, & \Delta \neq 0 \end{cases}$, $(l \in \mathbb{Z}^+)$. When $K - 2(M+P_{\mathrm{RS}})x < K-M-P_{\mathrm{RS}}$, combining (23)(b) with (23)(c), and using

$$\int_{u=b}^{a} (b-u)^c (u-a)^d du = -(b-a)^{c+d+1} \frac{c!d!}{(c+d+1)!}, \tag{31}$$

with $b < a$, $c, d \in \mathbb{N}$, $a = K$, $b = M + P_{\mathrm{RS}} + x$, $c = m-1$, and $d = m-1-r$, $g_1(x)$ is calculated as

$$\begin{aligned} g_1(x) = \frac{\lambda^m e^{-\lambda x}}{(m-1)!} \Bigg[& \sum_{r=0}^{m-1} \binom{m-1}{r} \alpha_r \lambda^{-r} \Big((x-K)^{m-1-r} \\ & + \lambda^m e^{-\lambda(M+P_{\mathrm{RS}})} \frac{(m-1-r)!}{(2m-1-r)!} (M+P_{\mathrm{RS}}+x-K)^{2m-1-r} \Big) \\ & - e^{-\lambda(M+P_{\mathrm{RS}}-K)} \pi(K) (M+P_{\mathrm{RS}}+x-K)^{m-1} \Bigg]. \end{aligned} \tag{32}$$

To obtain $g_2(x)$, I_4 in (23)(b) is rewritten as

$$\begin{aligned} I_4 = & \int_{u=M+P_{\mathrm{RS}}+x}^{K} B(x,u) g_0(u) du \\ & + \int_{u=M+P_{\mathrm{RS}}+x}^{K-M-P_{\mathrm{RS}}} B(x,u) (g_1(u) - g_0(u)) du, \end{aligned} \tag{33}$$

where $B(x,u) = (x-u+P_{\mathrm{RS}}+M)^{m-1} e^{-\lambda(M+P_{\mathrm{RS}}-u)}$.

By using the method of solving $g_1(x)$, when $K - 3(M+P_{\mathrm{RS}}) \le x < K-2(M+P_{\mathrm{RS}})$, one can obtain $g_2(x)$ as

$$\begin{aligned} g_2(x) = \frac{\lambda^m e^{-\lambda x}}{(m-1)!} \Bigg[& \sum_{r=0}^{m-1} \binom{m-1}{r} \alpha_r \lambda^{-r} \Big((x-K)^{m-1-r} \\ & + \lambda^m e^{-\lambda(M+P_{\mathrm{RS}})} \frac{(m-1-r)!}{(2m-1-r)!} (M+P_{\mathrm{RS}}+x-K)^{2m-1-r} \\ & + \lambda^{2m} e^{-2\lambda(M+P_{\mathrm{RS}})} \frac{(m-1-r)!}{(3m-1-r)!} (2(M+P_{\mathrm{RS}})+x-K)^{3m-1-r} \Big) \\ & - e^{-\lambda(M+P_{\mathrm{RS}})} e^{\lambda K} \pi(K) (M+P_{\mathrm{RS}}+x-K)^{m-1} - \lambda^m \\ & \times e^{-2\lambda(M+P_{\mathrm{RS}})} e^{\lambda K} \pi(K) (2(M+P_{\mathrm{RS}})+x-K)^{2m-1} \frac{(m-1)!}{(2m-1)!} \Bigg]. \end{aligned} \tag{34}$$

Similarly, for $n \ge 3$, one can get

$$\begin{aligned} g_n(x) = \frac{\lambda^m e^{-\lambda x}}{(m-1)!} \Bigg[& \sum_{z=0}^{n} \lambda^{zm} e^{-z\lambda(M+P_{\mathrm{RS}})} \sum_{r=0}^{m-1} \alpha_r \lambda^{-r} \binom{m-1}{r} \\ & \times \frac{(m-1-r)!}{((z+1)m-1-r)!} (z(M+P_{\mathrm{RS}})+x-K)^{(z+1)m-1-r} \\ & - \sum_{z=1}^{n} \lambda^{(z-1)m} e^{-z\lambda(M+P_{\mathrm{RS}})} e^{\lambda K} \pi(K) \\ & \times \frac{(m-1)!}{(zm-1)!} (z(M+P_{\mathrm{RS}})+x-K)^{zm-1} \Bigg]. \end{aligned} \tag{35}$$

Substituting $\pi(K)$ in (35), $g_n(x)$ can be written as

$$\begin{aligned} g_n(x) = e^{-\lambda x} \sum_{r=0}^{m-1} \frac{\alpha_r}{r!} \Bigg[& \sum_{z=0}^{n} \lambda^{(z+1)m-r} e^{-z\lambda(M+P_{\mathrm{RS}})} \\ & \times \frac{(z(M+P_{\mathrm{RS}})+x-K)^{(z+1)m-1-r}}{((z+1)m-1-r)!} \\ & - \sum_{z=1}^{n} \lambda^{zm} e^{-z\lambda(M+P_{\mathrm{RS}})} \frac{(z(M+P_{\mathrm{RS}})+x-K)^{zm-1}}{(zm-1)!} \Bigg]. \end{aligned} \tag{36}$$

When $0 \le x < P_{\mathrm{RS}}$, we set $g_p(x) = g(x)$. (37)(a) can be written as

$$g_p(x) = \frac{\lambda^m e^{-\lambda x}}{(m-1)!} \Bigg[\int_{u=0}^{x} (x-u)^{m-1} e^{\lambda u} g_p(u) du$$

$$g(x) = \begin{cases} \dfrac{\lambda^m e^{-\lambda x}}{(m-1)} \Bigg[\displaystyle\int_{u=0}^{x} (x-u)^{m-1} e^{\lambda u} g(u) du + x^{m-1} \int_{u=P_{\mathrm{RS}}}^{M+P_{\mathrm{RS}}} g(u) du \\ \quad + \displaystyle\int_{u=M+P_{\mathrm{RS}}}^{M+P_{\mathrm{RS}}+x} (x-u+P_{\mathrm{RS}}+M)^{m-1} e^{-\lambda(M+P_{\mathrm{RS}}-u)} g(u) du \Bigg], \quad 0 \le x < P_{\mathrm{RS}} & \text{(30a)} \\ g_0(x) - \dfrac{\lambda^m e^{-\lambda x}}{(m-1)} \Bigg[\underbrace{\displaystyle\int_{u=M+P_{\mathrm{RS}}+x}^{K} (x-u+P_{\mathrm{RS}}+M)^{m-1} e^{-\lambda(M+P_{\mathrm{RS}}-u)} g(u) du}_{I_4} \\ \quad + \pi(K) (x-K+P_{\mathrm{RS}}+M)^{m-1} e^{-\lambda(M+P_{\mathrm{RS}}-K)} \Bigg], \ P_{\mathrm{RS}} \le x < K-M-P_{\mathrm{RS}} & \text{(30b)} \\ \triangleq g_0(x) = \dfrac{\lambda^{m-r} e^{-\lambda x}}{(m-1)} \displaystyle\sum_{r=0}^{m-1} \binom{m-1}{r} (x-K)^{m-1-r} \alpha_r, \ K-M-P_{\mathrm{RS}} \le x < K. & \text{(30c)} \end{cases}$$

$$+x^{m-1}\left(\int_{u=P_{\mathrm{RS}}}^{K-l(M+P_{\mathrm{RS}})} g_l(u)du+\int_{u=K-l(M+P_{\mathrm{RS}})}^{M+P_{\mathrm{RS}}} g_{l-1}(u)du\right)+\int_{u=M+P_{\mathrm{RS}}}^{M+P_{\mathrm{RS}}+x}(x-u+P_{\mathrm{RS}}+M)^{m-1}e^{-\lambda(M+P_{\mathrm{RS}}-u)}g_{l-1}(u)du\Bigg]. \tag{37}$$

Let $I_S(x)=\frac{\lambda^m e^{-\lambda x}}{(m-1)!}\int_{u=0}^{x}(x-u)^{m-1}e^{\lambda u}g_p(u)du$ and

$$T(x)=\frac{\lambda^m e^{-\lambda x}}{(m-1)!}\Bigg[x^{m-1}\underbrace{\left(\int_{u=P_{\mathrm{RS}}}^{K-l(M+P_{\mathrm{RS}})} g_l(u)du+\int_{u=K-l(M+P_{\mathrm{RS}})}^{M+P_{\mathrm{RS}}} g_{l-1}(u)du\right)}_{T_{ab}}+\underbrace{\int_{u=M+P_{\mathrm{RS}}}^{M+P_{\mathrm{RS}}+x}(x-u+P_{\mathrm{RS}}+M)^{m-1}e^{-\lambda(M+P_{\mathrm{RS}}-u)}g_{l-1}(u)du}_{T_c}\Bigg], \tag{38}$$

(37) can be rewritten as

$$g_p(x)=T(x)+I_S(x). \tag{39}$$

Next, similar to the method for I_4, T_{ab} can be rewritten as

$$T_{ab}=\underbrace{\int_{u=P_{\mathrm{RS}}}^{M+P_{\mathrm{RS}}} g_{l-1}(u)du}_{T_a}+\underbrace{\int_{P_{\mathrm{RS}}}^{K-l(M+P_{\mathrm{RS}})} g_l(u)-g_{l-1}(u)du}_{T_b}. \tag{40}$$

$$\begin{aligned}T(x)=e^{-\lambda x}\sum_{r=0}^{m-1}\frac{\alpha_r}{r!}\Bigg[&\sum_{z=0}^{l-1}\lambda^m e^{-\lambda(z(M+P_{\mathrm{RS}})+P_{\mathrm{RS}})}\sum_{v=0}^{(z+1)m-1-r}\frac{(z(M+P_{\mathrm{RS}})+P_{\mathrm{RS}}-K)^{(z+1)m-1-r-v}x^{m-1}}{((z+1)m-1-r-v)!v!(m-1)!}\lambda^{(z+1)m-1-r-v}\gamma(v+1,\lambda M)\\
&-\sum_{z=1}^{l-1}\lambda^m e^{-\lambda(z(M+P_{\mathrm{RS}})+P_{\mathrm{RS}})}\sum_{v=0}^{zm-1}\frac{(z(M+P_{\mathrm{RS}})+P_{\mathrm{RS}}-K)^{zm-1-v}x^{m-1}}{(zm-1-v)!v!(m-1)!}\lambda^{zm-1-v}\gamma(v+1,\lambda M)\\
&+\lambda^m e^{-\lambda(l(M+P_{\mathrm{RS}})+P_{\mathrm{RS}})}\sum_{v=0}^{(l+1)m-1-r}\frac{(l(M+P_{\mathrm{RS}})+P_{\mathrm{RS}}-K)^{(l+1)m-1-r-v}x^{m-1}}{((l+1)m-1-r-v)!v!(m-1)!}\lambda^{(l+1)m-1-r-v}\gamma(v+1,\lambda(K-(l(M+P_{\mathrm{RS}})+P_{\mathrm{RS}})))\\
&-\lambda^m e^{-\lambda(l(M+P_{\mathrm{RS}})+P_{\mathrm{RS}})}\sum_{v=0}^{lm-1}\frac{(l(M+P_{\mathrm{RS}})+P_{\mathrm{RS}}-K)^{lm-1-v}x^{m-1}}{(lm-1-v)!v!(m-1)!}\lambda^{lm-1-v}\gamma(v+1,\lambda(K-(l(M+P_{\mathrm{RS}})+P_{\mathrm{RS}})))\\
&+\sum_{z=0}^{l-1}\lambda^{(z+2)m-r}e^{-\lambda(z+1)(M+P_{\mathrm{RS}})}\sum_{v=0}^{(z+1)m-1-r}\frac{((z+1)(M+P_{\mathrm{RS}})-K)^{(z+1)m-1-r-v}x^{m+v}}{((z+1)m-1-r-v)!(m+v)!}\\
&-\sum_{z=1}^{l-1}\lambda^{(z+1)m}e^{-\lambda(z+1)(M+P_{\mathrm{RS}})}\sum_{v=0}^{qm-1}\frac{((z+1)(M+P_{\mathrm{RS}})-K)^{zm-1-v}x^{m+v}}{(zm-1-v)!(m+v)!}\Bigg]\end{aligned} \tag{42}$$

$$\begin{aligned}d_{sr}=\frac{\lambda^s}{r!}\Bigg[&\sum_{z=0}^{l-1}e^{-\lambda(z(M+P_{\mathrm{RS}})+P_{\mathrm{RS}})}\sum_{v=0}^{(z+1)m-1-r}\frac{(z(M+P_{\mathrm{RS}})+P_{\mathrm{RS}}-K)^{(z+1)m-1-r-v}}{((z+1)m-1-r-v)!v!}\lambda^{(z+1)m-1-r-v}\gamma(v+1,\lambda M)\left(K^s+\lambda^m F_1(s)\right)\\
&-\sum_{z=1}^{l-1}e^{-\lambda(z(M+P_{\mathrm{RS}})+P_{\mathrm{RS}})}\sum_{v=0}^{zm-1}\frac{(z(M+P_{\mathrm{RS}})+P_{\mathrm{RS}}-K)^{zm-1-v}}{(zm-1-v)!v!}\lambda^{zm-1-v}\gamma(v+1,\lambda M)\left(K^s+\lambda^m F_1(s)\right)+e^{-\lambda(l(M+P_{\mathrm{RS}})+P_{\mathrm{RS}})}\\
&\times\sum_{v=0}^{(l+1)m-1-r}\frac{(l(M+P_{\mathrm{RS}})+P_{\mathrm{RS}}-K)^{(l+1)m-1-r-v}}{((l+1)m-1-r-v)!v!}\lambda^{(l+1)m-1-r-v}\gamma(v+1,\lambda(K-(l(M+P_{\mathrm{RS}})+P_{\mathrm{RS}})))\left(K^s+\lambda^m F_1(s)\right)\\
&-e^{-\lambda(l(M+P_{\mathrm{RS}})+P_{\mathrm{RS}})}\sum_{v=0}^{lm-1}\frac{(l(M+P_{\mathrm{RS}})+P_{\mathrm{RS}}-K)^{lm-1-v}}{(lm-1-v)!v!}\lambda^{lm-1-v}\gamma(v+1,\lambda(K-(l(M+P_{\mathrm{RS}})+P_{\mathrm{RS}})))\left(K^s+\lambda^m F_1(s)\right)\\
&-\sum_{z=0}^{l-1}\lambda^{zm}e^{-\lambda(z+1)(M+P_{\mathrm{RS}})}\sum_{v=0}^{s}\binom{s}{v}K^{s-v}v!\left(\lambda^{m-r}\frac{((z+1)(M+P_{\mathrm{RS}})-K)^{(z+1)m-r+v}}{((z+1)m-r+v)!}-\frac{((z+1)(M+P_{\mathrm{RS}})-K)^{zm+v}}{(zm+v)!}\right)\\
&+\sum_{z=0}^{l-1}\lambda^{(z+2)m-r}e^{-\lambda(z+1)(M+P_{\mathrm{RS}})}\sum_{v=0}^{(z+1)m-1-r}\frac{((z+1)(M+P_{\mathrm{RS}})-K)^{(z+1)m-1-r-v}}{((z+1)m-1-r-v)!}F_2(v,s)\\
&-\sum_{z=1}^{l-1}\lambda^{(z+1)m}e^{-\lambda(z+1)(M+P_{\mathrm{RS}})}\sum_{v=0}^{zm-1}\frac{((z+1)(M+P_{\mathrm{RS}})-K)^{zm-1-v}}{(zm-1-v)!}F_2(v,s)\Bigg],\end{aligned} \tag{44}$$

Substituting (36) in T_a, T_b and T_c, one can obtain

$$T_a = \sum_{r=0}^{m-1} \frac{\alpha_r}{r!} \Bigg[\sum_{z=0}^{l-1} e^{-\lambda(z(M+P_{\mathrm{RS}})+P_{\mathrm{RS}})} \sum_{v=0}^{(z+1)m-1-r} \frac{(z(M+P_{\mathrm{RS}})+P_{\mathrm{RS}}-K)^{(z+1)m-1-r-v}}{((z+1)m-1-r-v)!v!} \times \lambda^{(z+1)m-1-r-v}\gamma(v+1,\lambda M) - \sum_{z=0}^{l-1} e^{-\lambda(z(M+P_{\mathrm{RS}})+P_{\mathrm{RS}})} \times \sum_{v=0}^{zm-1} \frac{(z(M+P_{\mathrm{RS}})+P_{\mathrm{RS}}-K)^{zm-1-v}}{(zm-1-v)!v!} \lambda^{zm-1-v}\gamma(v+1,\lambda M) \Bigg], \tag{41a}$$

$$T_b = \sum_{r=0}^{m-1} \frac{\alpha_r}{r!} \Bigg[e^{-\lambda(l(M+P_{\mathrm{RS}})+P_{\mathrm{RS}})} \sum_{v=0}^{(l+1)m-1-r} \frac{(l(M+P_{\mathrm{RS}})+P_{\mathrm{RS}}-K)^{(l+1)m-1-r-v}}{((l+1)m-1-r-v)!v!} \times \lambda^{(l+1)m-1-r-v}\gamma(v+1,\lambda(K-(l(M+P_{\mathrm{RS}})+P_{\mathrm{RS}}))) \tag{41b}$$

$$\in I_{u=0}^{K} g(u)du + \pi(K) = \sum_{r=0}^{m-1} \frac{\alpha_r}{r!} \Bigg[\sum_{z=0}^{l-1} \lambda^m e^{-\lambda(z(M+P_{\mathrm{RS}})+P_{\mathrm{RS}})} \sum_{v=0}^{(z+1)m-1-r} \frac{(z(M+P_{\mathrm{RS}})+P_{\mathrm{RS}}-K)^{(z+1)m-1-r-v}}{((z+1)m-1-r-v)!v!} \lambda^{(z+1)m-1-r-v} \times \gamma(v+1,\lambda M)H_1 - \sum_{z=1}^{l-1} \lambda^m e^{-\lambda(z(M+P_{\mathrm{RS}})+P_{\mathrm{RS}})} \sum_{v=0}^{zm-1} \frac{(z(M+P_{\mathrm{RS}})+P_{\mathrm{RS}}-K)^{zm-1-v}}{(zm-1-v)!v!} \lambda^{zm-1-v}\gamma(v+1,\lambda M)H_1 + \lambda^m e^{-\lambda(l(M+P_{\mathrm{RS}})+P_{\mathrm{RS}})} \sum_{v=0}^{(l+1)m-1-r} \frac{(l(M+P_{\mathrm{RS}})+P_{\mathrm{RS}}-K)^{(l+1)m-1-r-v}}{((l+1)m-1-r-v)!v!} \lambda^{(l+1)m-1-r-v}\gamma(v+1,\lambda(K-(l(M+P_{\mathrm{RS}})+P_{\mathrm{RS}})))H_1 - \lambda^m e^{-\lambda(l(M+P_{\mathrm{RS}})+P_{\mathrm{RS}})} \sum_{v=0}^{lm-1} \frac{(l(M+P_{\mathrm{RS}})+P_{\mathrm{RS}}-K)^{lm-1-v}}{(lm-1-v)!v!} \lambda^{lm-1-v}\gamma(v+1,\lambda(K-(l(M+P_{\mathrm{RS}})+P_{\mathrm{RS}})))H_1 + \sum_{z=0}^{l-1} \lambda^{(z+2)m-r} e^{-\lambda(z+1)(M+P_{\mathrm{RS}})} \sum_{v=0}^{(z+1)m-1-r} \frac{((z+1)(M+P_{\mathrm{RS}})-K)^{(z+1)m-1-r-v}}{((z+1)m-1-r-v)!} H_2(v) - \sum_{z=1}^{l-1} \lambda^{(z+1)m} e^{-\lambda(z+1)(M+P_{\mathrm{RS}})} \sum_{v=0}^{zm-1} \frac{((z+1)(M+P_{\mathrm{RS}})-K)^{zm-1-v}}{(zm-1-v)!} H_2(v) + \sum_{z=0}^{l} e^{-\lambda(z(M+P_{\mathrm{RS}})+P_{\mathrm{RS}})} \sum_{v=zm}^{(z+1)m-1-r} \frac{(\lambda(z(M+P_{\mathrm{RS}})+P_{\mathrm{RS}}-K))^v}{v!} \Bigg], \tag{47}$$

$$b_r = \frac{1}{r!} \Bigg[\sum_{z=0}^{l-1} \lambda^m e^{-\lambda(z(M+P_{\mathrm{RS}})+P_{\mathrm{RS}})} \sum_{v=0}^{(z+1)m-1-r} \frac{(z(M+P_{\mathrm{RS}})+P_{\mathrm{RS}}-K)^{(z+1)m-1-r-v}}{((z+1)m-1-r-v)!v!} \lambda^{(z+1)m-1-r-v}\gamma(v+1,\lambda M)H_1 - \sum_{z=1}^{l-1} \lambda^m e^{-\lambda(z(M+P_{\mathrm{RS}})+P_{\mathrm{RS}})} \sum_{v=0}^{zm-1} \frac{(z(M+P_{\mathrm{RS}})+P_{\mathrm{RS}}-K)^{zm-1-v}}{(zm-1-v)!v!} \lambda^{zm-1-v}\gamma(v+1,\lambda M)H_1 + \lambda^m e^{-\lambda(l(M+P_{\mathrm{RS}})+P_{\mathrm{RS}})} \times \sum_{v=0}^{(l+1)m-1-r} \frac{(l(M+P_{\mathrm{RS}})+P_{\mathrm{RS}}-K)^{(l+1)m-1-r-v}}{((l+1)m-1-r-v)!v!} \lambda^{(l+1)m-1-r-v}\gamma(v+1,\lambda(K-(l(M+P_{\mathrm{RS}})+P_{\mathrm{RS}})))H_1 - \lambda^m e^{-\lambda(l(M+P_{\mathrm{RS}})+P_{\mathrm{RS}})} \sum_{v=0}^{lm-1} \frac{(l(M+P_{\mathrm{RS}})+P_{\mathrm{RS}}-K)^{lm-1-v}}{(lm-1-v)!v!} \lambda^{lm-1-v}\gamma(v+1,\lambda(K-(l(M+P_{\mathrm{RS}})+P_{\mathrm{RS}})))H_1 + \sum_{z=0}^{l-1} \lambda^{(z+2)m-r} e^{-\lambda(z+1)(M+P_{\mathrm{RS}})} \sum_{v=0}^{(z+1)m-1-r} \frac{((z+1)(M+P_{\mathrm{RS}})-K)^{(z+1)m-1-r-v}}{((z+1)m-1-r-v)!} H_2(v) - \sum_{z=1}^{l-1} \lambda^{(z+1)m} e^{-\lambda(z+1)(M+P_{\mathrm{RS}})} \sum_{v=0}^{zm-1} \frac{((z+1)(M+P_{\mathrm{RS}})-K)^{zm-1-v}}{(zm-1-v)!} H_2(v) + \sum_{z=0}^{l} e^{-\lambda(z(M+P_{\mathrm{RS}})+P_{\mathrm{RS}})} \sum_{v=zm}^{(z+1)m-1-r} \frac{(\lambda(z(M+P_{\mathrm{RS}})+P_{\mathrm{RS}}-K))^v}{v!} \Bigg]. \tag{53}$$

$$- e^{-\lambda(l(M+P_{\rm RS})+P_{\rm RS})} \sum_{v=0}^{lm-1} \frac{(l(M+P_{\rm RS})+P_{\rm RS}-K)^{lm-1-v}}{(lm-1-v)!v!}, \quad (41b)$$

$$T_c = \sum_{r=0}^{m-1} \frac{\alpha_r}{r!}(m-1)! \Bigg[\sum_{z=0}^{l-1} \lambda^{(z+1)m-r} e^{-\lambda(z+1)(M+P_{\rm RS})} \times \sum_{v=0}^{(z+1)m-1-r} \frac{((z+1)(M+P_{\rm RS})-K)^{(z+1)m-1-r-v} x^{m+v}}{((z+1)m-1-r-v)!(m+v)!} - \sum_{z=1}^{l-1} \lambda^{zm} e^{-\lambda(z+1)(M+P_{\rm RS})} \sum_{v=0}^{qm-1} \frac{((z+1)(M+P_{\rm RS})-K)^{zm-1-v} x^{m+v}}{(zm-1-v)!(m+v)!} \Bigg]. \quad (41c)$$

Substituting (41) into (38), one can get $T(x)$ as (42), as shown at the bottom of the p. 13. Then, one can obtain $g_p(x)$ as (37)(a). Next, we need to get the coefficients α_r. One defines

$$\alpha_s \triangleq \sum_{r=0}^{m-1} \alpha_r d_{sr} = \lambda^s [I_1(s) + I_2(s) + I_3(s) + (M+P_{\rm RS})^s e^{-\lambda(M+P_{\rm RS})} \sum_{r=0}^{m-1} \frac{\alpha_r}{r!}], \; s = 0, \ldots, m-1 \quad (43)$$

where $I_1(s) = \int_{u=0}^{P_{\rm RS}} (K-u)^s e^{\lambda u} g(u)du$, $I_2(s) = K^s \int_{u=P_{\rm RS}}^{M+P_{\rm RS}} g(u)du$, $I_3(s) = \int_{u=M+P_{\rm RS}}^{K} (K-u+P_{\rm RS}+M)^s e^{-\lambda(M+P_{\rm RS}-u)} g(u)du$.

Then, one can get d_{sr} as (44),as shown at the bottom of the p. 13
where

$$F_1(s) = \sum_{b=0}^{s} \binom{s}{b} (K-P_{\rm RS})^{s-b} \Bigg[\frac{b! {P_{\rm RS}}^{m+b}}{(m+b)!} + \frac{1}{m} \sum_{k=0}^{m-1} \Re \Bigg\{ e^{\lambda P_{\rm RS} e^{j\eta_k}} \left(\lambda e^{j\eta_k}\right)^{-(m+b)} \gamma\left(b+1, \lambda P_{\rm RS} e^{j\eta_k}\right) - \sum_{w=0}^{m-1} \frac{b! {P_{\rm RS}}^{w+b+1}}{(w+b+1)!} \left(\lambda e^{j\eta_k}\right)^{w-(m-1)} \Bigg\} \Bigg], \quad (45)$$

$$F_2(v,s) = \sum_{b=0}^{s} \binom{s}{b} (K-P_{\rm RS})^{s-b} \Bigg[\frac{b! {P_{\rm RS}}^{m+v+b+1}}{(m+v+b+1)!} + \frac{1}{m} \sum_{k=0}^{m-1} \Re \Bigg\{ e^{\lambda P_{\rm RS} e^{j\eta_k}} \left(\lambda e^{j\eta_k}\right)^{-(m+v+b+1)} \gamma\left(b+1, \lambda P_{\rm RS} e^{j\eta_k}\right) - \sum_{w=0}^{m+v} \frac{b! {P_{\rm RS}}^{w+b+1}}{(w+b+1)!} \left(\lambda e^{j\eta_k}\right)^{w-(m+v)} \Bigg\} \Bigg]. \quad (46)$$

Using $\int_{u=0}^{K} g(u)du + \pi(K) = 1$, one can get (47), as shown at the bottom of the previous page,

where

$$H_1 = \lambda^{-m} \Bigg[\frac{\gamma(m, \lambda P_{\rm RS})}{(m-1)!} + \frac{1}{m} \sum_{k=0}^{m-1} \Re\{\rho_{1k} - \sum_{w=0}^{m-1} \frac{e^{j\eta_k(w-(m-1))}}{w!} \gamma(w+1, \lambda P_{\rm RS}) \Bigg\} \Bigg], \quad (48)$$

$$H_2(v) = \lambda^{-(m+v+1)} \Bigg[\frac{\gamma(m+v+1, \lambda P_{\rm RS})}{(m+v)!} + \frac{1}{m} \sum_{k=0}^{m-1} \Re\{\rho_{2k} - \sum_{w=0}^{m+v} \frac{e^{j\eta_k(w-(m+v))}}{w!} \gamma(w+1, \lambda P_{\rm RS}) \Bigg\} \Bigg], \quad (49)$$

$$\rho_{1k} = \begin{cases} \frac{1-e^{-\lambda P_{\rm RS}\left(1-e^{j\eta_k}\right)}}{1-e^{j\eta_k}} e^{-j\eta_k(m-1)}, & k \neq 0 \\ \lambda P_{\rm RS}, & k = 0 \end{cases} \quad (50)$$

$$\rho_{2k} = \begin{cases} \frac{1-e^{-\lambda P_{\rm RS}\left(1-e^{j\eta_k}\right)}}{1-e^{j\eta_k}} e^{-j\eta_k(m+v)}, & k \neq 0 \\ \lambda P_{\rm RS}, & k = 0 \end{cases} \quad (51)$$

Let

$$\int_{u=0}^{K} g(u)du + \pi(K) \triangleq \sum_{r=0}^{m-1} \alpha_r b_r = 1, \quad (52)$$

where b_r can be obtained by (53), as shown at the bottom of the previous page.

Combining (43) with (52), we can obtain $\alpha_s + \sum_{r=0}^{m-1} \alpha_r (b_r - d_{sr}) = 1, s = 0, \ldots, m-1$, which is a non-homogeneous system of linear equations and it can be written as $\boldsymbol{\alpha} + \boldsymbol{A}\boldsymbol{\alpha} = \mathbf{1}$. The s-row and r-column expression for $\boldsymbol{A}$ can be expressed as $A_{sr} = b_r - d_{sr}$, which is detailed in (13).

REFERENCES

[1] C. Lin, G. Cai, T. Ning, and J. He, "A wireless-powered relaying system with energy buffer for implant WBAN," in *Proc. IEEE Conf. Int. Symp. Commun. Informat. Technol. (ISCIT)*, Xian, China, 2022, pp. 70–75.

[2] M. Gupta and B. S. Kumar, "Lightweight secure session key protection, mutual authentication, and access control (LSSMAC) for WBAN-assisted IoT network," *IEEE Sensors J.*, vol. 23, no. 17, pp. 20283–20293, Sep. 2023.

[3] J. Hu, G. Xu, L. Hu, S. Li, and Y. Xing, "An adaptive energy efficient MAC protocol for RF energy harvesting WBANs," *IEEE Trans. Commun.*, vol. 71, no. 1, pp. 473–484, Jan. 2023.

[4] J. Zhang and C. Dong, "Secure and lightweight data aggregation scheme for anonymous multi-receivers in WBAN," *IEEE Trans. Netw. Sci. Eng.*, vol. 10, no. 1, pp. 81–91, Feb. 2023.

[5] G. D. Ntouni, A. S. Lioumpas, and K. S. Nikita, "Reliable and energy-efficient communications for wireless biomedical implant systems," *IEEE J. Biomed. Health Informat.*, vol. 18, no. 6, pp. 1848–1856, Nov. 2014.

[6] J. Ding, E. Dutkiewicz, X. Huang, and G. Fang, "Energy-efficient distributed beamforming in UWB based implant body area networks," in *Proc. IEEE 81st Veh. Technol. Conf. (VTC)*, 2015, pp. 1–5.

[7] J. Cha, J. Choi, and D. J. Love, "Practical distributed reception for wireless body area networks using supervised learning," *IEEE Trans. Wireless Commun.*, vol. 21, no. 7, pp. 4898–4908, Jul. 2022.

[8] G. Cai, Y. Fang, J. Wen, G. Han, and X. Yang, "QoS-aware buffer-aided relaying implant WBAN for healthcare IoT: Opportunities and challenges," *IEEE Netw.*, vol. 33, no. 4, pp. 96–103, Jul. 2019.

[9] Y. Xiao, G. Cai, Y. Song, G. Cai, Y. Fang, and G. Han, "Performance analysis of buffer-aided relaying implant WBAN," in *Proc. IEEE Int. Symp. Med. Inf. Commun. Technol. (ISMICT)*, 2021, pp. 86–91.

[10] Y.-W. Chong, W. Ismail, K. Ko, and C.-Y. Lee, "Energy harvesting for wearable devices: A review," *IEEE Sensors J.*, vol. 19, no. 20, pp. 9047–9062, Oct. 2019.

[11] Y. Ma, Z. Luo, C. Steiger, G. Traverso, and F. Adib, "Enabling deep-tissue networking for miniature medical devices," in *Proc. IEEE Int. Conf. ACM Special Interest Group Data Commun.*, 2018, pp. 417–431.

[12] K. Chen, Z. Yang, L. Hoang, J. Weiland, M. Humayun, and W. Liu, "An integrated 256-channel epiretinal prosthesis," *IEEE J. Solid-State Circuits*, vol. 45, no. 9, pp. 1946–1956, Sep. 2010.

[13] G. C. McConnell, H. D. Rees, A. I. Levey, C.-A. Gutekunst, R. E. Gross, and R. V. Bellamkonda, "Implanted neural electrodes cause chronic, local inflammation that is correlated with local neurodegeneration," *J. Neural Eng.*, vol. 6, no. 5, Oct. 2009, Art. no. 056003.

[14] F. Akhtar and M. H. Rehmani, "Energy harvesting for self-sustainable wireless body area networks," *IT Prof.*, vol. 19, no. 2, pp. 32–40, Mar. 2017.

[15] F. Shabani, H. Philamore, and F. Matsuno, "An energy-autonomous chemical oxygen demand sensor using a microbial fuel cell and embedded machine learning," *IEEE Access*, vol. 9, pp. 108689–108701, 2021.

[16] H. Varghese, B. S. Athira, and A. Chandran, "Highly flexible tribo-electric nanogenerator based on PVDF nanofibers for biomechanical energy harvesting and telerehabilitation via human body movement," *IEEE Sensors J.*, vol. 23, no. 13, pp. 13925–13932, Jul. 2023.

[17] A. Sabovic, A. K. Sultania, C. Delgado, L. D. Roeck, and J. Famaey, "An energy-aware task scheduler for energy-harvesting batteryless IoT devices," *IEEE Internet Things J.*, vol. 9, no. 22, pp. 23097–23114, Nov. 2022.

[18] X. Ding, Z. Ying, W. Zu, and L. Han, "Experimental study on thermoelectric energy harvesting from indoor high-voltage disconnector," *IEEE Sensors J.*, vol. 24, no. 3, pp. 2985–2995, Feb. 2024.

[19] V. Singh and P. K. Upadhyay, "Cognitive hybrid satellite-terrestrial relay networks with simultaneous energy and information transmission," in *Proc. IEEE Adv. Netw. Telecommun. Syst. (ANTS)*, 2018, pp. 1–6.

[20] V. Singh, P. K. Upadhyay, D. B. da Costa, and U. S. Dias, "Hybrid satellite-terrestrial spectrum sharing systems with RF energy harvesting," in *Proc. IEEE Int. Conf. Pers., Indoor Mobile Radio Commun. (PIMRC)*, Bologna, Italy, 2018, pp. 306–311.

[21] Y. Xu, Z. Liu, C. Huang, and C. Yuen, "Robust resource allocation algorithm for energy-harvesting-based D2D communication underlaying UAV-assisted networks," *IEEE Internet Things J.*, vol. 8, no. 23, pp. 17161–17171, Dec. 2021.

[22] Z. Shi, H. Lu, X. Xie, H. Yang, C. Huang, J. Cai, and Z. Ding, "Active RIS-aided EH-NOMA networks: A deep reinforcement learning approach," *IEEE Trans. Commun.*, vol. 71, no. 10, pp. 5846–5861, Oct. 2023.

[23] T. Wang, Q. Xu, W. Jia, Z.-H. Mao, H. Tang, and M. Sun, "Dual-functional wireless power transfer and data communication design for micromedical implants," *IEEE J. Emerg. Sel. Topics Power Electron.*, vol. 9, no. 5, pp. 6259–6271, Oct. 2021.

[24] I. A. Shah, A. Basir, Y. Cho, and H. Yoo, "Safety analysis of medical implants in the human head exposed to a wireless power transfer system," *IEEE Trans. Electromagn. Compat.*, vol. 64, no. 3, pp. 640–649, Jun. 2022.

[25] G. Monti et al., "EMC and EMI issues of WPT systems for wearable and implantable devices," *IEEE Electromagn. Compat. Mag.*, vol. 7, no. 1, pp. 67–77, Apr. 2018.

[26] A. N. Abdulfattah, C. C. Tsimenidis, B. Z. Al-Jewad, and A. Yakovlev, "Performance analysis of MICS-based RF wireless power transfer system for implantable medical devices," *IEEE Access*, vol. 7, pp. 11775–11784, 2019.

[27] H. Mosavat-Jahromi, B. Maham, and T. A. Tsiftsis, "Maximizing spectral efficiency for energy harvesting-aware WBAN," *IEEE J. Biomed. Health Informat.*, vol. 21, no. 3, pp. 732–742, May 2017.

[28] L. Wang, F. Hu, Z. Ling, and B. Wang, "Wireless information and power transfer to maximize information throughput in WBAN," *IEEE Internet Things J.*, vol. 4, no. 5, pp. 1663–1670, Oct. 2017.

[29] D. Sui, F. Hu, W. Zhou, M. Shao, and M. Chen, "Relay selection for radio frequency energy-harvesting wireless body area network with buffer," *IEEE Internet Things J.*, vol. 5, no. 2, pp. 1100–1107, Apr. 2018.

[30] X. Zhang, K. Liu, and L. Tao, "A cooperative communication scheme for full-duplex simultaneous wireless information and power transfer wireless body area networks," *IEEE Sensor Lett.*, vol. 2, no. 4, pp. 1–4, Dec. 2018.

[31] S. Li, F. Hu, Z. Xu, Z. Mao, Z. Ling, and H. Liu, "Joint power allocation in classified WBANs with wireless information and power transfer," *IEEE Internet Things J.*, vol. 8, no. 2, pp. 989–1000, Jan. 2021.

[32] M. M. Sandhu, S. Khalifa, R. Jurdak, and M. Portmann, "Task scheduling for energy-harvesting-based IoT: A survey and critical analysis," *IEEE Internet Things J.*, vol. 8, no. 18, pp. 13825–13848, Sep. 2021.

[33] R. Morsi, D. S. Michalopoulos, and R. Schober, "Performance analysis of near-optimal energy buffer aided wireless powered communication," *IEEE Trans. Wireless Commun.*, vol. 17, no. 2, pp. 863–881, Feb. 2018.

[34] D. Bapatla and S. Prakriya, "Performance of a cooperative network with an energy buffer-aided relay," *IEEE Trans. Green Commun. Netw.*, vol. 3, no. 3, pp. 774–788, Sep. 2019.

[35] D. Bapatla and S. Prakriya, "Performance of energy-buffer aided incremental relaying in cooperative networks," *IEEE Trans. Wireless Commun.*, vol. 18, no. 7, pp. 3583–3598, Jul. 2019.

[36] D. Bapatla and S. Prakriya, "Performance of a cooperative communication network with green self-sustaining nodes," *IEEE Trans. Green Commun. Netw.*, vol. 5, no. 1, pp. 426–441, Mar. 2021.

[37] D. Bapatla and S. Prakriya, "Performance of two-hop links with an energy buffer-aided IoT source and a data buffer-aided relay," *IEEE Internet Things J.*, vol. 8, no. 6, pp. 5045–5061, Mar. 2021.

[38] A. Celik, K. N. Salama, and A. M. Eltawil, "The Internet of Bodies: A systematic survey on propagation characterization and channel modeling," *IEEE Internet Things J.*, vol. 9, no. 1, pp. 321–345, Jan. 2022.

[39] A. Vyas, S. Pal, and B. K. Saha, "Relay-based communications in WBANs: A comprehensive survey," *ACM Comput. Surveys*, vol. 54, no. 1, pp. 1–34, May 2021.

[40] J. Wang and Q. Wang, *Body Area Communications: Channel Modeling, Communication Systems, and EMC*. Hoboken, NJ, USA: Wiley, 2012.

[41] A. K. Teshome, B. Kibret, and D. T. H. Lai, "A review of implant communication technology in WBAN: Progress and challenges," *IEEE Rev. Biomed. Eng.*, vol. 12, pp. 88–99, 2019.

[42] T. Ninikrishna, A. Preethi, and Z. Mishra, "Optimal wireless power transfer techniques for passive deep brain stimulation devices," in *Proc. IEEE Int. Conf. Innovat. Technol. (INOCON)*, 2020, pp. 1–5.

[43] A. Basir and H. Yoo, "Efficient wireless power transfer system with a miniaturized quad-band implantable antenna for deep-body multitasking implants," *IEEE Trans. Microw. Theory Techn.*, vol. 68, no. 5, pp. 1943–1953, May 2020.

[44] A. Abdi and H. Aliakbarian, "A miniaturized UHF-band rectenna for power transmission to deep-body implantable devices," *IEEE J. Transl. Eng. Health Medic.*, vol. 7, pp. 1–11, 2019.

[45] S. Roy, A. N. M. W. Azad, S. Baidya, M. K. Alam, and F. Khan, "Powering solutions for biomedical sensors and implants inside the human body: A comprehensive review on energy harvesting units, energy storage, and wireless power transfer techniques," *IEEE Trans. Power Electron.*, vol. 37, no. 10, pp. 12237–12263, Oct. 2022.

[46] S. J. Ambroziak et al., "An off-body channel model for body area networks in indoor environments," *IEEE Trans. Antennas Propag.*, vol. 64, no. 9, pp. 4022–4035, Sep. 2016.

[47] A. Abdi and M. Kaveh, "On the utility of Gamma PDF in modeling shadow fading (slow fading)," in *Proc. IEEE Conf. Veh. Technol.*, 1999, pp. 2308–2312.

[48] A. Abdi, H. Barger, and M. Kaveh, "A simple alternative to the lognormal model of shadow fading in terrestrial and satellite channels," in *Proc. IEEE Conf. Veh. Technol.*, 2001, pp. 2058–2062.

[49] A. Abdi and M. Kaveh, "A comparative study of two shadow fading models in ultrawideband and other wireless systems," *IEEE Trans. Wireless Commun.*, vol. 10, no. 5, pp. 1428–1434, May 2011.

[50] J. B. Lee, Y. Rong, L. Gopal, and C. W. R. Chiong, "Mutual information maximization for SWIPT AF MIMO relay systems with non-linear EH models and imperfect channel state information," *IEEE Trans. Veh. Technol.*, vol. 71, no. 8, pp. 8503–8518, Aug. 2022.

[51] E. Boshkovska, D. W. K. Ng, N. Zlatanov, A. Koelpin, and R. Schober, "Robust resource allocation for MIMO wireless powered communication networks based on a non-linear EH model," *IEEE Trans. Commun.*, vol. 65, no. 5, pp. 1984–1999, May 2017.
[52] S. A. Tegos, P. D. Diamantoulakis, A. S. Lioumpas, P. G. Sarigiannidis, and G. K. Karagiannidis, "Slotted ALOHA with NOMA for the next generation IoT," *IEEE Trans. Commun.*, vol. 68, no. 10, pp. 6289–6301, Oct. 2020.

TING NING received the B.Sc. degree in electronic and information engineering from Hunan City University, Yiyang, China, in 2021. She is currently pursuing the M.Sc. degree in communication engineering with the Guangdong University of Technology, Guangzhou, China. Her primary research interests include wireless body area networks, NOMA networks, and the Internet of Things.

CAN LIN received the B.Sc. degree in communication engineering from Ludong University, Shandong, China, in 2020 and the M.S. degree in communication engineering from the Guangdong University of Technology, Guangzhou, China, in 2023. His primary research interests include wireless body area networks and the Internet of Things.

GUOFA CAI (Senior Member, IEEE) received the B.S. degree in communication engineering from Jimei University, Xiamen, China, in 2007, the M.S. degree in circuits and systems from Fuzhou University, Fuzhou, China, in 2012, and the Ph.D. degree in communication engineering from Xiamen University, Xiamen, China, in 2015. In 2017, he was a Research Fellow with the School of Electrical and Electronic Engineering, Nanyang Technological University, Singapore. He is currently an Associate Professor with the School of Information Engineering, Guangdong University of Technology, China. His primary research interests include information theory and coding, spread-spectrum modulation, wireless body area networks, and Internet of Things.

KENGYUAN XIE received the B.Sc. degree in electronic and information engineering from the Dongguan University of Technology, Dongguan, China, in 2021. He is currently pursuing the M.Sc. degree in information and communication engineering with the Guangdong University of Technology, Guangzhou, China. His primary research interests include spread-spectrum modulation, reconfigurable intelligent surface, and Internet of Things.

JIGUANG HE (Senior Member, IEEE) received the Ph.D. degree in communications engineering from the University of Oulu, Finland, in 2018. He currently serves as a Senior Researcher with the Technology Innovation Institute, Abu Dhabi, UAE, and holds a Docentship (also known as an Adjunct Professor) with the University of Oulu. From September 2013 to March 2015, he was affiliated with the State Key Laboratory of Terahertz and Millimeter Waves, City University of Hong Kong, focusing on beam tracking within millimeter-wave MIMO systems. Subsequently, from June 2015 to August 2021, he was associated with the Centre for Wireless Communications, the University of Oulu, initially as a Doctoral Researcher and later as a Postdoctoral Researcher. He served as an Assistant Professor with the Macau University of Science and Technology from August 2021 to March 2022. He has actively contributed to numerous international and national projects, including EU FP7 RESCUE, EU H2020 ARIADNE, and the 6G Flagship, and received one FDCT-GDST joint research project from Macau Science and Technology Development Fund. His research interests span integrated sensing and communications, reconfigurable intelligent surfaces, millimeter-wave MIMO communications, and advanced signal processing techniques. He received the Best Paper Award from IEEE ICCT 2023. He is recognized as an Exemplary Reviewer for IEEE TRANSACTIONS ON COMMUNICATIONS and IEEE COMMUNICATIONS LETTERS, and he serves as a Technical Program Committee Member for various IEEE conferences. He is currently serves as an Associate Editor for IEEE TRANSACTIONS ON VEHICULAR TECHNOLOGY.

CHONGWEN HUANG (Member, IEEE) received the B.Sc. degree from Nankai University in 2010, the M.Sc. degree from the University of Electronic Science and Technology of China in 2013, and the Ph.D. degree from the Singapore University of Technology and Design in 2019, where he was a Postdoctoral from October 2019 to September 2020. In September 2020, he joined the Zhejiang University as a Tenure-Track Young Professor. His main research interests are focused on holographic MIMO surface/reconfigurable intelligent surface, B5G/6G wireless communications, mmWave/THz communications, and deep learning technologies for wireless communications. He is the recipient of 2021 IEEE Marconi Prize Paper Award, 2023 IEEE Fred W. Ellersick Prize Paper Award, and 2021 IEEE ComSoc Asia–Pacific Outstanding Young Researcher Award. Since 2021, he has served as an Editor for IEEE COMMUNICATIONS LETTER, *Elsevier Signal Processing*, *EURASIP Journal on Wireless Communications and Networking*, and *Physical Communication*.

MÉROUANE DEBBAH (Fellow, IEEE) is a Professor with the Khalifa University of Science and Technology, Abu Dhabi, and the Founding Director of the KU 6G Research Center. He is a Frequent Keynote Speaker with international events in the field of telecommunication and AI. In the Communication field, he has been at the heart of the development of small cells (4G), Massive MIMO (5G), and Large Intelligent Surfaces (6G) technologies. In the AI field, he is known for his work on Large Language Models, distributed AI systems for networks and semantic communications. His research has been lying at the interface of fundamental mathematics, algorithms, statistics, information and communication sciences with a special focus on random matrix theory, and learning algorithms. He received the multiple prestigious distinctions, prizes, and best paper awards (more than 40 IEEE best paper awards) for his contributions to both fields and according to research.com is ranked as the best scientist in France in the field of Electronics and Electrical Engineering. He is a WWRF Fellow, a Eurasip Fellow, an AAIA Fellow, an Institut Louis Bachelier Fellow, and Member émérite SEE.